Influence of shoreface morphological changes since the 19th century on nearshore hydrodynamics and shoreline evolution in Wissant Bay (northern France)

Alexa Latapy, Arnaud Héquette, Amandine Nicolle, Nicolas Pouvreau

Version of Record: https://www.sciencedirect.com/science/article/pii/S0025322719304670
Manuscript_4c44f119014803271502eea8f7d800da

Influence of shoreface morphological changes since the 19th century on nearshore hydrodynamics and shoreline evolution in Wissant bay (northern France)

Alexa Latapy[a,*], Arnaud Héquette[a], Amandine Nicolle[b], Nicolas Pouvreau[c]

[a] *Laboratoire d'Océanologie et de Géosciences, University Littoral Côte d'Opale, Univ. Lille, CNRS, UMR 8187, LOG, 62930 Wimereux,France*
[b] *ENSTA Bretagne, 2 rue François Verny, 29806 Brest Cedex 09, France*
[c] *SHOM, 13 Rue du Châtellier CS92803, 29228 Brest CEDEX 02, France*

Abstract

Located at the southern approaches to the North Sea, the Wissant bay has had the most rapidly eroding shoreline in mainland France in recent decades. Using historical bathymetries spanning the second half of the 19th century to the present, an analysis of the long-term coastal morphological changes and evolution of a prominent sand bank (Line bank) extending across the bay was carried out. A period of overall seabed erosion with a width-reduction of the Line bank; a deepening of the channel between the Line bank and the coast; and a lowering of the foreshore have been ongoing since the middle of the 20th century. This phase followed a period of channel infill in the western part of Wissant bay in the early 20th century. Numerical modelling of wave propagation and tidal circulation was performed using the TELEMAC suite of models to get some insights into the influence of these bathymetry changes on coastal hydrodynamics. Two seabed configurations were identified revealing a contrasting hydrodynamic circulation. An erosional one induces an acceleration of tidal currents and an increase in wave height. Conversely, accumulation leads to an hydrodynamic regime weakening with a decrease in current velocity and to

*Corresponding author
Email addresses: alexa.latapy@gmail.com (Alexa Latapy), arnaud.hequette@univ-littoral.fr (Arnaud Héquette), amandine.nicolle@ensta-bretagne.fr (Amandine Nicolle), nicolas.pouvreau@shom.fr (Nicolas Pouvreau)

more wave energy dissipation in the nearshore. This study highlights the role of morphological feedbacks between nearshore morphology and coastal hydrodynamics. The identification of these feedbacks mechanisms at a historical time scale is important to assess potential drivers of coastal changes.

Keywords: Sand banks, North Sea, France, Hydrodynamic, Tidal currents, Waves, Wissant bay

---

1. Introduction

Sand banks are large sedimentary features that occur in many coastal and shelf seas where there is a large amount of sediment and strong enough currents to transport this sediment (Caston, 1972; Kenyon et al., 1981; Dyer & Huntley, 1999; Deleu et al., 2004; Pan et al., 2007). There is a complex interaction between hydrodynamic and seabed leading to a variety of shapes and sizes, classified according to their formation and hydrodynamic settings (Huthnance, 1982; Dyer & Huntley, 1999; de Swart & Yuan, 2018). These sand banks are controlled either by storms (storm-generated ridges) or by tidal currents (tide-dominated banks) (Belderson, 1986)

The southern North Sea is characterized by a large number of tidal sand banks and has been extensively studied (Houbolt, 1968; Caston, 1972; Davies, 1980; Lanckneus et al., 1992; Berné et al., 1994; Lanckneus et al., 1994; Tessier et al., 1999) Sand banks play an important role in influencing shoreline evolution by attenuating the incident wave energy through wave breaking and bed friction processes (MacDonald & O'Connor, 1996; Héquette & Aernouts, 2010). Erosion is widespread along the central and southern part of the North Sea coastline, in France 20% of the coasts are under erosion (Hédou et al., 2018). In Wissant bay (northern France) the average shoreline retreat can exceed 5 m.an^{-1} (Aernouts & Héquette, 2006; CEREMA, 2018). Previous studies have suggested strong interactions between shoreline evolution and associated nearshore due to cross-shore and long-shore sediment transfers (Carter et al., 1982; Hanna & Cooper, 2002; Shaw et al., 2008; Héquette et al., 2009; Héquette & Aernouts, 2010;

Thomas et al., 2011; Héquette et al., 2013; Sedrati & Anthony, 2014).

Long bathymetric time series (several decades to centuries) are rare and generally localised in the vicinity of ports or in the context of dredging and aggregate extraction operations. In northern France, topographic and hydrographic surveys of coastal and nearshore morphologies have been conducted since the beginning of the 19th century and provide a direct source of data for assessing coastal and nearshore environments evolution (Latapy et al., 2019). Understanding the long-term characteristics of the morphology and the association with natural and anthropogenic forcing factors are important for coastal management. Historical bathymetries have already been used to investigate coastal morphology and hydrodynamic interactions (Cooper & Navas, 2004; Bertin, 2005; Bertin & Chaumillon, 2005; Aernouts & Héquette, 2006; Horrillo-Caraballo & Reeve, 2008; Héquette & Aernouts, 2010). For example, Horrillo-Caraballo & Reeve (2008) demonstrated that the 150 year-long changes in UK's eastern sand bank morphology can be largely explained by changes in its tidal residual currents. Cooper & Navas (2004) simulated wave propagation across the southeast coast of Northern Ireland and found a marked change in nearshore patterns of energy dispersal and related sediment transport pathways in one century. Nevertheless, these investigations generally focused on wave or tide-induced processes whereas natural systems are subjected to a combination of waves and tides. Indeed, tides change the mean water depth, which affects wave propagation over the inner shelf and the shoreface (Wolf & Prandle, 1999; Osuna & Monbaliu, 2004). Tides are also responsible for variations in the nearshore flow field which in turn modifies wave-current interaction (Wolf & Prandle, 1999), especially in a macrotidal environment. In addition, interactions between wave generated currents and tidal currents lead to an increase of bottom shear stress, particularly at the sand bank crests that can intensify sediment transport (Villaret & Davies, 2004; Giardino et al., 2010; Brown et al., 2015).

The present investigation tries to quantify the relative importance of nearshore morphology changes on wave and tide interactions and analyzes the possible impacts on shoreline evolution since the 19th century. First, the coastal evolution

of Wissant bay was assessed using historical bathymetry by comparison of digital bathymetric data. Then, effects of the tide-induced time-varying water depths and currents on wave height, and their possible changes depending of the sea bed evolution, were investigated. Finally, the links between documented shoreline changes and modelled modifications in tidal currents and wave regime in the coastal zone are also discussed.

2. Study area

2.1. Wissant bay's shoreface morphology

The North Sea coast of France generally consists of wide, gently sloping, sandy barred beaches (Reichmüth & Anthony, 2007). Sand banks are particularly widespread in this area, where they form linear shore-parallel or slightly oblique sand bodies about 10–30 km long and 1–3 km wide. These banks belong to the Flemish Banks (Houbolt, 1968) and generally occur as groups of banks from shallow coastal areas near beaches to depths of several tens of meters (Vicaire, 1991; Anthony & Orford, 2002). Previous studies have revealed a strong variability in nearshore evolution along large parts of the northern France's coastal zone since the last few decades (Aernouts & Héquette, 2006; Héquette et al., 2013) but also over a larger time-scale (Aernouts, 2005; Ruz et al., 2017; Latapy et al., 2019).

Wissant bay is 8 km-long and located on the westernmost part of the French North Sea coast (Figure 1). It forms a well defined, single longshore sediment cell between Capes Gris Nez and Blanc Nez (Dewez et al., 1989; Beck et al., 1991; Anthony, 2000; Anthony et al., 2006). It is characterized by a 300 to 600 m-wide intertidal bar-trough beach dissected by drainage channels (Sedrati & Anthony, 2007). The gently sloping shallow shoreface extending seaward of the beach bars and trough is characterized by a prominent tidal sand bank named the Line bank (Figure 1), oriented WSW-ENE, roughly parallel to the coastline. The Line bank belongs to headlands banks based on the categorization by Dyer & Huntley (1999) and particularly banner banks formed where the coast changes

direction and where headland are resistant to erosion. The sediment distribution consists of a remarkably homogeneous sand, with median diameter (D_{50}) ranging from 0.17 to 0.21 mm (Anthony & Héquette, 2007; Sedrati & Anthony, 2007).

Massive aggregate extraction has been carried out in the past, especially in the western sector of the Line bank, closest to the shore. A Senate report mentions that during the 1970s, about 600 000 m^3 of sediment was extracted (Pintat, 1975). This practice was prohibited in 1983, but the damages caused by this extraction, added to other anthropogenic causes such as the expansion of the port of Boulogne-sur-mer in the 1930s, has resulted in a significant sediment deficit in the bay. This recurrent sediment deficit now affects the beach which contributes to the shoreline retreat (Crapoulet et al., 2017). Indeed Wissant bay is presently one of the most strongly eroded coasts in mainland France, erosion is strongest in the southwestern and central parts of the bay while the northeast was characterized by a significant foredune growth during the second part of the 20th century (Aernouts & Héquette, 2006; Chaverot et al., 2008; Sedrati & Anthony, 2014) (Figure 1a).

2.2. Hydrodynamic context

As with adjacent coastal area, the Wissant bay is a typical mixed storm-wave and tide-dominated environment. This bay is subject to a complex pattern of time-varying influences of both tides and storms and even to wind forced flows (Héquette et al., 2008). Winds are generally from southwest and northeast, but the strongest winds mostly originate from west to southwest.Based on the HOMERE wave hindcast database (Accensi & Maisondieu, 2015), offshore waves are commonly less than 1 m (mean Hs = 0.87 m) but may exceed 3 m during extreme events (max Hs = 4.5 m). Wave periods mostly range from 5 to 7 seconds (mean period 6.14 s) and the dominant waves are from the south-west to west (from the English Channel) followed by waves from the northeast to north (originated from the North Sea) (Figure 1b). Because depth-induced refraction and dissipation of waves occurs over the shoreface and over the Line bank, at the coast waves are usually reduced and from a NW to NNE window.

The tidal regime is semi-diurnal and macrotidal (tidal range about 7 m during spring tides (Shom, 2017)). The nearshore circulation during fair-weather conditions is characterized by a flood-dominated asymmetry responsible for strong northeastward-directed currents (Héquette et al., 2008) (Figure 1c). Longshore currents can become particularly strong during storms as a result of direct wind and wave stress (Sedrati & Anthony, 2007). The net regional sediment transport in the coastal zone is directed eastward in response to the easterly-directed, flood-dominated tidal circulation (Augris et al., 1990) but locally counter-drift currents toward the west-southwest are also observed (EGIS, 2014).

3. Methodology

3.1. Bathymetry changes

Several bathymetry datasets covering the northern France coastline and adjoining seabed are available dating back to the mid-19th century. Most surveys were carried out over 2-3 years given the limited resources available at the time and the extent of the area covered (Table 1). Historic hydrographic field sheets from the French Hydrographic Service (SHOM) were scanned, digitized and then interpolated using the "krigging" method to produce Digital Elevation Models (DEMs). The coordinate system is the WGS84, and elevations are in meters below chart datum (lowest low-water spring level). The uncertainty associated with each survey was calculated by taking into account the sounding tool and the positioning technique (Table 1). To quantify bathymetry changes, differential DEMs, along-shore and cross-shore transects and sediment volume calculation were made (more details on interpolation and computing methods can be found in Latapy et al. (2019)). Morphological changes and computed volumes are considered significant when they are not within the error margin.

3.2. Numerical model

To investigate the influence of seabed morphological changes on coastal hydrodynamic, a numerical approach was developed. This study used the

TELEMAC suite of models, consisting of TELEMAC-2D (Hervouet, 2007) and TOMAWAC to simulate tides and waves respectively. As a first step, TELEMAC-2D and TOMAWAC were run separately to study individually the impact of bathymetric changes on tidal circulation and on wave propagation.

Subsequently, TELEMAC-2D and TOMAWAC were run in fully coupled mode so that the wave propagation module integrates the effects of the time-varying water depth and currents computed by the circulation modules. TELEMAC transfers to TOMAWAC values of current velocities and water depths, while TOMAWAC solves the wave action density conservation equation with reference to those current and water depth values and returns to TELEMAC the updated values of the wave driving forces FX and FY (including surface, bottom and radiation stresses) acting on the current. Water-depths variation modulates the dissipation of waves energy by bottom friction and wave breaking. Opposing tidal flows induce a steepening of the incident wave field thus increasing wave height. Finally, the combination of the time-varying water depths and currents leads to wave refraction and to a variability of the incident wave energy at specific coastal locations.

TELEMAC-2D and TOMAWAC were set up on a domain covering northern France's coastal zone - from the Belgium border to the Dover Strait (Figure 9). The first three bathymetry surveys extended over sufficiently large areas were used for numerical modelling (2016 survey was restricted to Wissant bay) (Table 1). DEMs generated from the selected bathymetry surveys were used to obtain three grids (Table 2) with a mesh resolution ranging from 250 m at the coast and over sand banks, increasing to 2.5 km offshore (Figure 9).

We forced our model to simulate the most powerful currents and waves possible in each mesh in order to identify high energy areas and those that have potentially undergone the most significant changes. We focussed our analysis on extreme events because coastal changes (such as beach and coastal dune erosion) are largely due to high-energy processes (Masselink et al., 2014; Castelle et al., 2015). Forcing conditions are described in the following sections.

3.2.1. TELEMAC forcing

The model is forced at the offshore open boundary with specified elevation for 143 tidal harmonics from the tidal model cstFRANCE developed and used by the SHOM (Le Roy & Simon, 2003). The validation of the models was carried out with tidal observations and predictions at the ports of Calais and Dunkirk. Current observations also allowed the model to be adjusted and calibrated (see the Appendix A for a detailed overview of the validation of the model). The time step is set to 10 seconds and the bottom friction coefficient is computed with Chezy's law. As the modelled area was spatially restricted, and is composed of quasi-homogeneous sea-bed sediment (sandy-gravelly) (Anthony & Héquette, 2007) a uniform friction coefficient was applied to the entire mesh (64 $m^{1/2}$.s). This coefficient is consistent with those obtained for equivalent surficial sediment(Soulsby, 1983, 1997; Cooper et al., 2004).

The model was run for a period of 30 days during the highest astronomical tides of 2015 (03/01/2015 to 03/30/2015) with sea-level elevation over the whole domain at 10 min intervals. Residual tidal currents are computed over the whole simulated period, these maps were used to identify possible transport pathways. Since the maps represent flow and not sediment transport they are only indicative of the likely direction of sediment transport and should not be interpreted quantitatively.

3.2.2. TOMAWAC parametrization

TOMAWAC model enables us to evaluate the effects of changing seabed morphology on wave refraction and on the pattern of wave energy distribution at the coast (see the Appendix B for a detailed overview of the validation of the model). Significant wave height (Hs), peak wave period (Tpeak) and wave direction (Dir) were calculated using TOMAWAC spectral wave model run on the same mesh as the hydrodynamic calculation (Figure 9) with a time step of 10 seconds, 20 frequency bins and 20 wave directions. Observations from a wave buoy located offshore (CEREMA, 1985) and analysis of hindcase database in this area (Boudière et al., 2013; Accensi & Maisondieu, 2015) showed a strongly bi-

model distribution of wave direction grouped around north-easterly and westerly directions (Figure1b). A set of two wave model runs were created by applying constant wave height, peak period and directions boundary forcing using the 99th percentile of wave height calculated from HOMERE database (Hs99%) for each of the two dominant wave directions. The model was run for these two wave conditions representative of the extreme wave regime of the region. (see Table 3).

4. Results

4.1. Evolution of the Wissant bay seabed

The bathymetric differential maps between 1878 and 2016 allowed us to examine the evolution of the seabed morphology in the Wissant bay (Figure 2). Significant bathymetry changes have occurred all over the study area since the end of the 19th century. An extended seafloor lowering of more than 7 m has taken place on both sides of the Line bank and also in the westernmost part of the foreshore. Moreover, an erosion pattern is clearly identified offshore of the Line bank in the northern part of the bay. Conversely, significant sediment accumulation has only been observed on the NE of the Line bank. Based on the bathymetry change observed and the error margin of ± 2.7 m between these two dates, an estimate of the volume change was computed showing a significant loss of more than 28 x 10^6 m^3 of sediment throughout the bay. Considering only the Line bank, this loss is estimated at 14 x 10^6 m^3. In order to analyze the Line bank and nearby morphological evolution, cross-shore and long-shore profiles were derived from DEMs (Figure 3), which revealed two distinct periods of evolution:

- Between 1878 and 1910: on the westernmost and central part of the bay, the Line bank underwent a lowering of its crest and a simultaneous widening (Profile A and B on Figure 3), especially towards the coast. This coastward migration led to a infill of the channel between the coast and the sand bank, which is well-identified on Profile A. On Profile C, the

onshore migration of the Line bank is visible, although the channel remained unchanged in the easternmost part of the Wissant bay. Profile D confirms the lowering of the crest over almost the total bank area. The foreshore rose (Profile A) or remained stable (Profiles B and C) between the end of the 19th and the beginning of the 20th century. The associated bathymetric differential map (Figure 2 inset map) shows that over almost the whole bay, morphological changes were relatively minor. It indicates a stability of the coastal zone to the east and sediment accumulation to the west during this period.

- Between 1910 and 2016: the channel between the coast and the Line bank was subject to significant erosion, with more than 5 m lowering on Profile A. Conjointly, the Line bank experienced a decrease of its width of about 500-600 m (Profile B) and up to 700 m locally (Profile A). The most remarkable changes are visible on Profile B, in 1974 the Line bank did not exceed a width of 200 m. In 1974, the height of the bank was at its lowest level (Profile A and D) while the eastern part of the bay was more stable. Over the 1974-2016 period, even though the Line bank experienced a slight increase of its width (Profile B), in most part of the Wissant bay, the channel continued to deepen and reached the -5 m isobath on Profile A and -12 m on Profile C. This had an impact on the foreshore which lowered significantly during the 20th century in the western and central part of the bay (Profile A and B) while Profile C indicates a more stable morphology.

Therefore, until the beginning of the 20th century, Wissant bay had experienced an infilling of coastal channel, mostly due to the widening and the onshore migration of the Line bank in the western and central part of the bay. It was during the 20th century that a widespread erosion of the bay can be observed. It not only impacts on the Line bank's morphology, but also the channel and the foreshore - leading to a net landward retreat of the shoreline observed during the second half of the 20th century (Aernouts & Héquette, 2006; CEREMA,

2018).

Because wave energy distribution at the coast strongly depends on wave refraction and dissipation over the shoreface, any change in the nearshore morphology is expected to modify wave propagation patterns and therefore induce changes in wave height. In this macrotidal environment, tide must be taken into account in the model in order to also study the effects of water level variation on wave energy. Results of these simulations are presented in the following sections (Section 4.2 and 4.3).

4.2. Tidal residual currents changes

Figure 4 shows the computed tidally induced residual currents for Wissant bay over a 30-day simulation for three bathymetry configurations (1878, 1910, 1974). In Figure 5 the model integrates the wave propagation module suggesting a complex residual current flow field that is partly controlled by wave direction.

4.2.1. 1878

Considering the no-waves configuration, tidal residual currents are essentially directed to the NE which correspond to the flood-dominated direction and can reach 0.3 $m.s^{-1}$on the seaward side of the Line bank (Figure 4a).

With waves from the N-NE direction, the intensity of residual currents is generally of the same amplitude as that of the no-waves configuration, although the distribution of these velocities changes: with weaker currents on the offshore side and more intense to the interior of the bay (Figure 5a). Locally, and mostly on the east of the bay, current direction is also reversed, with residual currents towards the SW, which correspond to a predominance of the ebb.

WSW waves tend to induce much stronger residual currents (Figure 5d) with speeds ranging from 0 to 0.9 $m.s^{-1}$; the maximum residual currents being located on the seaward flank of the Line bank (residual current peak at 0.9 $m.s^{-1}$). In this configuration, currents are mainly directed towards the NE, which would be expected given the initial wave direction that would drive and intensify the currents in Wissant bay.

4.2.2. 1910

By not taking into account any waves, an area of high current velocities (about 0.5 $m.s^{-1}$) is noticeable on the western border of the model, probably due to boundary effect in the model (Figure 4b). Across Wissant bay, tidal residual currents are directed towards the NE, except in the westernmost part where onshore currents are apparent. Throughout the foreshore, residual currents are weaker than those computed in the 1878 mesh. In the NE part of the Line bank, there is also a decrease in the velocity of residual currents.

When waves are from the NE sector, as in the 1878 model, there is a residual current direction reversal in the eastern part of the foreshore leading to a local predominance of the ebb (Figure 5b). On the SW part of Wissant bay, currents are weaker, not only at the foreshore, but also at or near the crest of the Line bank (0.12 $m.s^{-1}$).

For westerly waves, over the whole bay, currents are stronger than the two previous set-ups. However, residual currents are lower over the 1910 bathymetry compared to currents velocities observed with westerly waves over the 1878 bathymetry. This is clearly observable, even on the seaward side of the sand bank where currents are usually more intense, they do not exceed 0.75 $m.s^{-1}$ against 0.9 $m.s^{-1}$ in 1878 (Figure 5e).

4.2.3. 1974

With the no-waves set-up, residual currents mostly flow toward the NE (flood-direction) (Figure 4c). Weakest currents are located on the central part of the Line bank ($\approx$ 0.05 $m.s^{-1}$), while strongest ones, are located in the SW part of the bay, particularly on the seaward side of the bank ($\approx$ 0.3 $m.s^{-1}$).

For northeasterly waves, residual currents speeds are lower at the sand bank margins ($<$ 0.1 $m.s^{-1}$) but they increase on the Line bank crest. At the shoreline, the linear area where currents are directed towards the SW is extended north-eastward and now reaches the town of Wissant. Facing the hamlet of Wissant, these SW residual currents are opposed to those in the channel and may create shearing zones (Figure 5c).

With westerly waves, residual current are still stronger than those obtained with the no-waves and NE-waves configurations (Figure 5f). However, compared to the 1910-W set-up, areas where currents exceed 0.4 $m.s^{-1}$ are more extensive, especially in the western part of the bay (on the top of the Line bank and also in the channel). Likewise, there is an increase in velocities on the Line bank seaward flank and at the shoreline in the central part of the bay.

4.3. Impact on waves propagation

Wave height transects from the 1878, 1910 and 1974 models are presented in Figures 6 for northeasterly waves and in Figure 7 for westerly waves (the location of the wave height transects is the same as the bathymetric ones). In each transect, for same wave conditions, the wave heights obtained during high water springs and without considering tides are plotted in order to compare the effect of tides on wave height distribution and in turn energy dissipation in the nearshore.

Figures 6 and 7 clearly show the effect of tides on wave height with higher wave heights occurring during high water springs. These results are consistent with previous studies that investigated the contribution of tidal modulation on incident wave power (Peregrine, 1976; Lugo-Fernández et al., 1998; Masselink, 1998; Davidson et al., 2008; Hedges, 2015). There is a strong wave energy dissipation over the sand bank for both westerly and northeasterly waves, which results in a similar Hs distribution from one configuration to another as shown on Profile A, B and C (Figures 6 and 7).

On the top of the Line bank, wave height changed significantly between 1878 and 1974 (Profile D Figures 6 and 7). Without tides, in the 1878 model, there is already a strong gradient, with an Hs of 1.5 m in the NE part of the bay decreasing until 0 m to the SW. However, from 1878 onwards, waves exceed 0.5 m on the Profile D over a length of 4 km in 1878, increasing to 6 km in 1910, and finally 7.5 km in 1975, which corresponds approximately to the length of the Line bank (Profile D Figures 6 and 7). At the end of the 19th century, the Line bank was locally above the hydrographic datum (Profile A Figure 3)

so it was often emerged inducing wave dissipation and breaking. This explain why, without tides, in the 1878 and even in the 1910 model, Hs is equal to 0 m from the top of the bank to the coast (Profile A Figures 6 and 7). However, during high water springs, the water depth is high enough to cover the Line bank and waves can break farther landward (Profile A Figures 6 and 7). When high water springs are considered, on the NE part of the Profile D, Hs slightly increases in time but remained mostly stable for both western and northeastern waves. However, significant changes occurred in the western and central part of the Line bank where, for both waves direction, an increase Hs of around 0.5 m is observed between the 1878 and the 1974 models (Profiles A and B Figures 6 and 7).

From 1878 to 1974, waves do not only become higher on the top of the sand bank, but also in most part of the coastal channel. This increase is well-identified in Profiles D and E (Figures 6 and 7) where Hs become larger particularly in the central part of the profiles. At the end, in 1974, without tides, more than 4 km of channel recorded a wave height greater than 0.5 m (against 2 km in 1878 and 3 km in 1910). During high water springs, for all models, Hs exceeds 0.5 m over the whole channel. In the same way, the portion of the profile greater than 1 m represents 66% for 1878, 60% for 1910 and 83% for 1974 revealing a small decrease of wave energy in the channel in 1910 and a strong rise in 1974 (Profile E Figures 6 and 7).

From 1878 to 1974, in the western and central part of Wissant bay, there is an increase in wave height at the coast of 0.2-0.4 m for W waves and of 0.3-0.6 m for NE waves for both non-tidal and high water springs configurations (Profile A et B Figures 6 and 7). The highest wave heights are logically observed during high water springs due to higher water levels over the bank and shoreface, this being particularly visible on Profile B. With a lower water depth (no tide) the wave height strongly decrease landward in 1878 and 1910 but when the water level is higher (high water springs), wave height decreases gradually (Figures 6 and 7). On Profile B, this results in a strong reduction of Hs between the channel and the coast (over less than 500 m) highlighting strong wave energy

dissipation at the coast.

The easternmost part of Wissant bay is characterized by different wave height changes, becoming more stable and even reducing locally between the 1878, 1910, and 1974 models (Profile C Figures 6 and 7). In Profile C, wave height changes are less significant. It should be noted, that for the 1974 model, with or without tides, the wave height is always lower than the ones obtained with the 1878 and 1910 models. Considering the tide, however, in 1974, waves are higher offshore up to X=2000 (isobath -5 m) and only lower from the foreshore to the shoreline (Profile C Figures 6 and 7)

In summary, the results of our numerical modeling wave height over successive bathymetries since 1878 suggest that morphological changes and Line bank positions, have induced significant changes in wave height distribution (Table 7) along Wissant's coast. Accordingly, we can divide Wissant bay into three main areas (Table 7):

- The eastern part of the bay, characterized by a stability in wave heights through time, and even a decreasing trend in some areas.
- The central part of the bay where our results show a generally increased wave heights between the Line bank and the coast from 1878 to 1974.
- The western part of the bay, with a more complex evolution: between 1878 and 1910, wave height increased on the Line bank, but decreased on the foreshore and the shoreline, while an overall increasing trend of wave height is observed all along the nearshore for the period 1910-1974.

5. Discussion

Based on historical bathymetric surveys, our study reveals a high variability in the Wissant bay seabed morphology. Using ancient nautical charts, Briquet's work (Briquet, 1930) pointed out that the Line bank was once located more offshore from Wissant Bay and has experienced a gradually on-shore migration since 1640 (Figure 8). In 1776, the bank was located 800 m seaward of the Gris

Nez Cape at low tide, but was at only 200 m from the cape in 1810. In 1835, the area between the bank and the coast was largely exposed at low tide, although a deep channel was still present. Briquet's work highlighted that the trough was gradually filled in the 1870s, and in 1910 the Line bank was almost welded to the beach, which is confirmed in the western part of the Wissant bay by our DEMs (Profile A Figure 3). Previous studies and our historical bathymetry sets enable us to assess the complex morphological evolution of this area:

- During the end of the 19th and the beginning of the 20th century, the Line bank experienced a widening and a coastward migration resulting in a gentler beach and foreshore profile in 1910;

- Since the 1970s, Wissant bay underwent a thinning of the Line bank, a deepening of the coastal channel and a lowering of the foreshore associated with an overall erosion of the seabed. It appears that the lowering of the seabed in Wissant Bay is a fairly recent phenomenon following a phase of sediment accumulation and coastward migration of the bank.

Nearshore changes are strongly linked to shoreline evolution as shown by several other studies carried out in a variety of coastal settings (Corbau et al., 1999; McNinch, 2004; Aernouts & Héquette, 2006; Backstrom et al., 2007; Houser et al., 2008) and the recent shoreline retreat observed in the western and central part of the bay and the shoreline advance in the eastern part can be partially explained by this interaction (Aernouts & Héquette, 2006).

With a similar approach, Bertin (2005); Horrillo-Caraballo & Reeve (2008) found that the pattern of residual currents is strongly linked to the configuration of sand banks. In addition, observations and numerical results on sandy coast revealed the essential role of wave energy dispersal in the nearshore sediment distribution (Morton et al., 1995; Sedrati & Anthony, 2007) and its contribution for controlling the development of erosion or accretion hot spots.(Barnard & Hanes, 2006; Héquette & Aernouts, 2010)

The results of our numerical modeling highlight two types of shoreface/nearshore

configurations leading to two different types of hydrodynamic circulation presented below.

5.1. The eroding-configuration

The 1974 model can be assimilated as the **eroding-configuration**. For this bathymetric configuration, stronger residual tidal currents, and higher wave heights are observed in the western and central part of the Line bank, compared to the two preceding seabed morphologies. This occurs for waves either from the W or NE (Figures 5, 6 and 7). The last DEMs highlight a significant thinning of the Line bank and an extensive lowering of the seabed in Wissant Bay between 1910 and 1974 (Figure 2). This contributes to increase the foreshore's exposure to high energy waves by reducing the effects of wave dissipation and refraction on the sea bed (Barnard & Hanes, 2006). This may have also modified wave-induced sand dynamics (due to wave-current interaction) and thus sand bank equilibrium. Sediment transported from the nearshore to the upper shoreface is more likely to be remobilized and distributed northeastward by currents than to accumulate on the beach. This combined phenomenon may have induced an increase in longshore sediment transport that could explain the pervasive shoreline retreat observed in the second half of the 20th century (Aernouts & Héquette, 2006; Sedrati & Anthony, 2014). Moreover, the wave-current shearing zones in front of Wissant town obtained with the NE-waves configuration (Figure 5c) could accentuate the erosion of the channel and the beach in this area (Jing & Ridd, 1996). In the eastern part of Wissant bay, the foreshore experienced a decrease of Hs and also a reduction of the strength of residual currents directed to the SW. This reduction in current speeds may result in less sediment transport to the western and central parts of the Wissant bay that could enhance the sediment deficit in these parts of the bay. On the other hand, it may also result in more sediment deposition in the eastern part of the bay and therefore generate the shoreline advance observed in this part of the bay during the second half of the 20th century.

5.2. The accumulation-configuration

The **accumulation-configuration** (corresponding to the 1910 bathymetric configuration), reveals significant changes in the central and western parts of the bay. First, during NE-waves events, residual currents are weaker than in 1878 between the Line bank and the coast where current speeds do not exceed 0.15 $m.s^{-1}$ (Figure 5b). For western waves, residual currents remain strong on the seaward side of the Line bank, but have decreased in the channel and on the foreshore compared to 1878 (Figure 5e). Secondly, the increasing wave height between 1878 and 1910 on the top of the Line bank (Profile D Figures 6 and 7) and the following decrease of Hs in the channel (Profile E Figures 6 and 7) indicate wave energy dissipation. As shown in several studies, gently sloping dissipative profiles favor onshore-directed transport (Hesp, 1988; Davidson-Arnott & N. Law, 1996; Aagaard et al., 2004; Cooper & Navas, 2004; Héquette & Aernouts, 2010). Modelling of wave propagation revealed that the widening and the onshore movement of the Line bank between 1878 and 1910 was responsible for a decrease in wave energy associated with more dissipative conditions in the nearshore zone, which may have resulted in a net, wave-induced shoreward sediment transport. In this configuration, as residual currents speeds are particularly lower in the western and central part of the bay, this may have favored sediment accumulation and channel infill.

Beach and nearshore morphologies are the result of the interaction between physical processes controlling the cross-shore and longshore transport that eventually cause morphological changes. The present study highlights positive feedbacks between hydrodynamic and coastal morphology. Indeed, both bathymetric configurations (eroding and accumulation) affect the hydrodynamic circulation in such a way that the morphodynamic response may be reinforced. However, our analysis do not identify processes that can induce a switch between both regimes. According to their dynamic and morphological characteristics, sandy beaches can be classified into several morphodynamic types (Wright & Short, 1984; Short, 1999). Scott et al. (2011) expanded this classification to take into account the influence of tidal range. In their classification, Wissant

bay belongs to the MITB beach type (Multiple inter-tidal barred). Investigation made on MITB beaches suggest that these beaches have a rapid morphological response under increasing energy conditions, while under decreasing energy the adjustment is slower. Owever, because our study is essentially focussed on extreme events, it does not examine relaxation time effects. Nevertheless, a decrease or increase in storms frequency, variations in large-scale hydrodynamic circulation and/or changes in sediment supply through time may have affected the nearshore-shoreface equilibrium and then induced a morphodynamic reversal.

5.3. Combined effects of waves and tides

It appears from these different simulation runs that, residual currents obtained do not exceed 0.40 $m.s^{-1}$ and are mostly directed in the flood-direction (*i.e.* to the NE) when tides only are considered. The interaction with the waves, on the contrary, accelerate these currents (up to 0.9 $m.s^{-1}$ locally for western waves) and sometimes even reverse their direction (with NE waves). These results are consistent with King et al. (2019) study which investigate the relative influence of tidal and wave forcing on potential sand transport in analogous macrotidal environment (South West UK). Similarly, they found that extreme waves are able to induce directional shifts and even full reversals which strongly influence sand transport direction. Likewise, although the direction of the wave has only a limited influence on the wave height at the coast, taking into account the tides affects the water elevation and therefore, in the case of high water springs, nearshore wave height may double or even triple. This shows the potential importance and influence of these processes on shoreline dynamic. Individually, they already provide some preliminary explanations for the observed shoreline changes, but when coupled together, a very energetic hydrodynamism emerges in this sector, which has evolved considerably over the past century.

5.4. Limitations of the results and perspectives for future research

In this study, one of the main assumptions made was that past and present hydrodynamics remained the same. Accordingly, the only variable would be the

seabed morphology as the main task of this study was to highlight the influence of nearshore morphology changes on wave and tide interactions. In fact, wave climate has potentially changed since the beginning of the 20th century. Using a 100-year numerical wind-wave hindcast, Dodet et al. (2010); Bertin et al. (2013) found an increase of wave height of 0.01 m.year^{-1} in the North-East Atlantic Ocean since 1900 due to a rise in wind speed of more than 20%. At a global scale, with a 23-year database of altimeter measurements (1985-2009), Young et al. (2011) investigated global changes in wave height. They suggested an increase of more than 1%.year^{-1} in the 99th-percentile wave height trends over this period at high latitudes. The rate of increase is greater for extreme events as compared to the mean condition. Moreover, MacDonald & O'Connor (1996) predicted an average wave energy increasing by the order of 10% by 2130 under a sea level rise scenario. On European shelf, Idier et al. (2017) investigated the effect of sea level rise on tidal dynamics and observed a notable increase in high tide levels in the Southern part of the North Sea. All these studies suggest significant changes in hydrodynamic circulation. Sea level rise was not taken into account in our numerical models, but added to the increase in wave height during the 20th century, one can imagine that the hydrodynamic context at the end of the 19th century was weaker and therefore that our 1878 and 1910 models partially overestimate currents and waves. Potentially, it is possible that the differences in energy levels between the end of the 19th century and 1974 may be even greater than expected. Finally, in the present context of climate change, even if coastal morphology remained hypothetically unchanged in the following decades, it can be expected that there will be significant changes in coastal hydrodynamics in this area with the increase in wave height with sea level rise.

Hydrodynamic circulation changes have an important role in the coastal systems equilibrium. However, it is also important to assess the sediment in transit through this system, which should be included in any further work. It is frequently suggested that the recent trend reversal is not only due to natural causes but also to local factors related to anthropogenic development or con-

struction (Mattheus et al., 2018; Li et al., 2019), such as the expansion of the port of Boulogne-sur-mer in the 1930s and the massive aggregate extraction in the 1960s-1970s. The construction of the Boulogne-sur-mer dikes may have reduced or even blocked the sedimentary transit from the English Channel coasts to the North Sea, thus reducing the supply to the Bay of Wissant. In addition, the extraction of marine aggregate in the western of the bay and on the Line Bank, the sediment budget being in deficit, may have triggered a process of erosion that became self-maintained even following the interruption of extraction (Sedrati & Anthony, 2014).

Other studies carried out in the northern France's coastal zone have revealed that sand banks are actively migrating alongshore and onshore as a result of shore-parallel tidal currents and onshore storm waves (Garlan, 1990; Corbau, 1995; Tessier et al., 1999; Héquette et al., 2009; Héquette & Aernouts, 2010; Héquette et al., 2013) . Other studies carried out in the inner part of some continental shelves have highlighted significant variations in nearshore morphologies due to sand banks dynamics (Parker et al., 1982; De Moor, 2002; Hanna & Cooper, 2002; Schmitt & Mitchell, 2014). This numerical approach, being based upon general principle of hydrodynamics is anticipated to have wider applicability to others nearshore sandbank systems, as those previously mentioned. This will contribute to a better understanding of the long-term dynamics of this coastal zones, characterized by the presence of mobile sand banks, and provide a better insight into the mechanisms involved in their evolution.

6. Conclusion

Changes in the Wissant bay nearshore have been investigated directly from a comparison of historical hydrographic surveys determined from seabed soundings as well as with the results from an hydrodynamic model. This model, coupling both tides and waves, for the northern France area (between the Dover Strait and the Belgium border) has been calibrated and validated. In the second half of the 20th century, the nearshore experienced a thinning of the Line bank,

a deepening of the coastal channel and a lowering of the foreshore leading to an overall erosion of the seabed. This phase followed a period of channel infill in the western part of the bay in the early 1910s.

These recent morphological changes led to significant hydrodynamic shift with residual tidal currents acceleration in most parts of the nearshore zone and an increase of wave height in the western and central parts of Wissant bay where one of the most rapid shoreline retreats has been recorded in France since the 1950s. However, at the beginning of the 20th century, seabed morphology led to more dissipative conditions: it resulted in an overall decrease in wave height and to lower residual currents speeds that could favor sediment deposition on the foreshore and eventually on the beach. As the seabed morphology changes, this affects tidal currents and wave dissipation; so there is a complex interaction and feedback between hydrodynamic circulation and the seabed. Using historical bathymetry coupling with numerical models has provided a qualitative explanation of observed bathymetry changes and shoreline evolution during the last decades. This approach involves wave-current interactions and brings new insight into the long-term coastal dynamics of this area and on the processes controlling erosion and accumulation along shorelines affected by the movement of nearshore sand banks.

7. Acknowledgements

The first author (A.L) was funded by the Université du Littoral Côte d'Opale (ULCO) through a PhD fellowship. Hydrographic field sheets are stored at SHOM's archives and used in this study, thanks to the hosting agreement SHOM-ULCO (n°133/2016). The authors would like to acknowledge the DDTM 62 (French departmental direction of territories and the sea) for providing the available 2016 bathymetry survey and current measurements in the study area. A part of the digitization and interpolation phase was made by Jean-Baptiste Robin-Chanteloup during his 6-month internship in SHOM. The authors thank Thierry Gendrier and Matthieu Bastien for their invaluable assistance in the

researching of hydrographic archives and their interpretations and Jonathan Genevier for help with the ScanBathy software. The authors thank Peter Magee for proofreading this article. We gratefully acknowledge the constructive comments provided by three anonymous reviewers who helped to improve the quality of the manuscript. Raw data can be found from the corresponding author at alexa.latapy@gmail.com

Appendix A. TELEMAC-2D validation

TELEMAC-2D (v6p3) solve the non-conservative form of the shallow water equations (Equations A.1, A.2 and A.3):

$$\frac{\partial h}{\partial t} + \mathbf{U}.\nabla(h) + h.div(\mathbf{U}) = S_h \tag{A.1}$$

$$\frac{\partial U}{\partial t} + \mathbf{U}.\nabla(U) = -g\frac{\partial h}{\partial x} + S_x + \frac{1}{h}div(h\nu_t \nabla U) \tag{A.2}$$

$$\frac{\partial V}{\partial t} + \mathbf{U}.\nabla(V) = -g\frac{\partial h}{\partial y} + S_y + \frac{1}{h}div(h\nu_t \nabla V) \tag{A.3}$$

where h is the water depth, t is the time, $\mathbf{U}$ is the depth-averaged velocity vector with components U and V in the x and y Cartesian coordinate respectively. ν_t is the diffusion coefficient (considered as constant), g is the gravity acceleration, S_h is a source or sink term in the continuity equation. The source or sink term S_x and S_y in the dynamic equations represent the wind and the atmospheric pressure, the Coriolis force, the bottom friction and additional sources or sink of momentum within the domain in the two directions x and y. Model domains are shown in Figure 9 and integrate historical bathymetry (1878-79, 1910-11, 1930-32 and 1974-76). To validate the tidal model, a range of cases were studied. A set of tests was performed in which the bottom friction coefficient was changed by varying the Chezy's law coefficient between 50 and 70 $m^{1/2}$.s. The influence of the bottom friction coefficient on the models ability to reproduce observed data was examined first. A set of tidal height observations are available for Dunkirk and Calais harbors at each date and are used to compare with outputs of our 4 models (Figure10b). Tidal height predictions are also compared with results from numerical models to only evaluate astronomical tides. Bests results are obtained using a coefficient of 64 $m^{1/2}$.s. Soulsby (1983, 1997)'s works on dynamics of marine sands linked the Chezy coefficient to the nature of the seabed. For sandy-gravelly seabed(Anthony & Héquette, 2007), Chezy coefficient ranges between 57 and 65 which is consistent with our results.

The Table 5 shows tidal height comparison at Calais and Dunkirk (tidal observation are only available in 1878 and 1930); it appears that for each models, simulated results and tide predictions give a good correlation ($R^2 > 0.85$). By analysing observations and models, R^2 obtained are also statistically significant even if these values are lower than those computed with predictions. This deviation is probably due to meteorological phenomena (atmospheric pressure, wind effect) recorded in water levels but not taken into account in the model parametrization. Only a few tidal current records are available in model areas before the 1970s, however, in 1935, current observations were made at Calais and are then used to improve the calibration our models. It appears that with a coefficient of 64 $m^{1/2}$.s, model currents amplitude and phase are consistent with observations made in 1935 (Figure 10a). A statistically significant correlation is obtained with a R^2=0.95. Simulations were carried out over a winter period (March 2015), *i.e.* when the water-column is well mixed, no thermocline is present and therefore no vertical stratification is required.

Appendix B. TOMAWAC validation

TOMAWAC models the changes, both in time and in the spatial domain, of the power spectrum of wind-driven waves and wave agitation. The directional spectrum of wave action density is considered as a function of five variables (Marcos, 2003):

$$N(\overrightarrow{x}, \overrightarrow{k}, t) = N(x, y, k_x, k_y, t) \tag{B.1}$$

Where $\overrightarrow{x} = (x, y)$ is the spatial location in a Cartesian coordinate system, $\overrightarrow{k} = (k_x, k_y) = (k.sin\Theta, k.cos\Theta)$ is the wave number vector for directional spectrum discretization,Θ is the wave propagation direction and t the time. Hypotheses made on the wave representation, on the model application domain and on modelled physical processes enable to write the evolution of the directional spectrum of wave action as followed:

$$N(k_x, k_y, x, y, t) = \frac{CCg}{2\pi\sigma}\tilde{N}(x, y, f_r, \Theta, t) \tag{B.2}$$

Cg and C are respectively the group velocity and the phase velocity of waves and σ is the angular frequency. The equation expresses that, in the general case of waves propagating in a non-homogeneous, unsteady environment (currents and/or sea levels varying in time and space), the wave action is preserved to within the source and sink terms (designated by the term Q)(Marcos, 2003). Our study area is mainly located in the coastal zone, so we configured our model for the coastal domain. For shallow areas, some physical processes must be included and specified in our parameter file such as:

- Bottom friction-induced dissipation (Qbf), with Qbf=0.038 $m^2.s^{-3}$ which improves the estimation of wave growth in shallow water (Zijlema et al., 2012).
- Non-linear triad interactions between waves, considering the LTA (Lumped Triad Approximation) which improves the computation time.
- Bathymetric breaking-induced dissipation (Qbr) where we have chosen the Battjes and Janssen's model (1978) after performing a sensitivity test between the 4 proposed models in TOMAWAC (Battjes and Janssen, Thornton and Guya, Roelvink, and Izumiya and Horikawa).

The TOMAWAC wave model was first run independently. In the absence of wave observations before the 1970s, the model was validated from another wave model (WaveWatchIII). WaveWatchIII has been implemented on the MANGAS grid (created by Michaud et al. (2015)), which is an unstructured grid with a resolution ranging from 10 km at the open boundaries of the domain to about 200 m resolution at the coast. The mesh is based on the HOMONIM digital elevation model (DEM) developed by SHOM as part of the HOMONIM project (Biscara et al., 2014). In order to compare the same bathymetry, we created a new grid based on the HOMONIM DEM and we simulated the two offshore waves configuration (Table 3). Then, results obtained with TOMAWAC are compared to those of Wavewatch with similar wave conditions (Table 6).

For westerly and northeasterly waves, Hs obtained with WaveWatchIII and TOMAWAC were extracted at each node (Figure 11a-b). The distribution of Hs was compared using Q-Q plot. Regression coefficient obtained are very close to 1 and error terms are close to 0, which confirms the model's ability to reproduce Hs of WW3 (Figure 11c-d). Largest differences are observed for Hs between 0 and 1 m. These differences are mainly due to the fact that WW3 considers additional forcing, such as wind, tide and currents in contrast to TOMAWAC. Overall, we obtain for both simulations an RMSE of less than 0.15 m corresponding to an error of less than 6% and an R^2 of 0.96-0.97 which is statistically significant (Figure 11c-d).

References

Aagaard, T., Davidson-Arnott, R., Greenwood, B., & Nielsen, J. (2004). Sediment supply from shoreface to dunes: linking sediment transport measurements and long-term morphological evolution. *Geomorphology*, *60*, 205–224. URL: http://www.sciencedirect.com/science/article/pii/S0169555X03003325. doi:10.1016/j.geomorph.2003.08.002.

Accensi, M., & Maisondieu, C. (2015). HOMERE. Ifremer - Laboratoire Comportement des Structures en Mer. URL: https://doi.org/10.12770/cf47e08d-1455-4254-955e-d66225c9dc.

Aernouts, D. (2005). *Le rôle des changements bathymétriques à l'avant-côte sur l'évolution des littoraux meubles du Cap Gris-Nez à Dunkerque, Côte d'Opale, Nord de la France*. Ph.D. thesis Université Littoral Côte d'Opale. URL: http://www.theses.fr/2005DUNK0138.

Aernouts, D., & Héquette, A. (2006). L'évolution du rivage et des petits-fonds en baie de Wissant pendant le XXe siècle (Pas-de-Calais, France). *Géomorphologie: relief, processus, environnement*, *12*, 49–64. URL: https://geomorphologie.revues.org/477. doi:10.4000/geomorphologie.477.

Anthony, E., & Orford, J. (2002). Between Wave- and Tide-Dominated Coasts: the Middle Ground Revisited. *Journal of Coastal Research Special Issue*, *36*, 8–15. doi:10.2112/1551-5036-36.sp1.8.

Anthony, E. J. (2000). Marine sand supply and Holocene coastal sedimentation in northern France between the Somme estuary and Belgium. *Geological Society, London, Special Publications*, *175*, 87–97. URL: http://sp.lyellcollection.org/content/175/1/87. doi:10.1144/GSL.SP.2000.175.01.08.

Anthony, E. J., & Héquette, A. (2007). The grain-size characterisation of coastal sand from the Somme estuary to Belgium: Sediment sorting processes and mixing in a tide-and storm-dominated setting. *Sedimentary Geology*,

202, 369–382. URL: http://www.sciencedirect.com/science/article/pii/S0037073807001364. doi:10.1016/j.sedgeo.2007.03.022.

Anthony, E. J., Vanhee, S., & Ruz, M.-H. (2006). Short-term beach–dune sand budgets on the north sea coast of France: Sand supply from shoreface to dunes, and the role of wind and fetch. *Geomorphology*, *81*, 316–329. URL: http://www.sciencedirect.com/science/article/pii/S0169555X06001577. doi:10.1016/j.sedgeo.2007.03.022.

Augris, C., Clabaut, P., & Vicaire, O. (1990). Le domaine marin du Nord-Pas de Calais. Nature, morphologie et mobilité des fonds.

Backstrom, J. T., Jackson, D. W. T., & Cooper, J. A. G. (2007). Shoreface Dynamics of Two High-Energy Beaches in Northern Ireland. *Journal of Coastal Research*, *ICS2007*, 5. URL: https://www.jstor.org/stable/26481656.

Barnard, P. L., & Hanes, D. M. (2006). Integrating field research, modeling and remote sensing to quantify morphodynamics in a high-energy coastal setting, ocean beach, San Francisco, California. URL: https://pubs.er.usgs.gov/publication/70028957. doi:10.1061/40855(214)96.

Beck, C., Clabaut, P., Dewez, S., Vicaire, O., Chamley, H., Augris, C., Hoslin, R., & Caillot, A. (1991). Sand bodies and sand transport paths at the English Channel-North Sea border: Morphology, hydrodynamics and radioactive tracing. *Oceanologica Acta, Special issue*, . URL: http://archimer.ifremer.fr/doc/00268/37887/.

Belderson, R. H. (1986). Offshore Tidal and Non-Tidal Sand Ridges and Sheets: Differences in Morphology and Hydrodynamic Setting, . (pp. 293–301). URL: http://archives.datapages.com/data/cspg_sp/data/011/011001/293_cspgsp0110293.htm.

Berné, S., Trentesaux, A., Stolk, A., Missiaen, T., & de Batist, M. (1994). Architecture and long term evolution of a tidal sandbank: The Middelkerke Bank (southern North Sea). *Marine Geol-*

ogy, *121*, 57–72. URL: http://www.sciencedirect.com/science/article/pii/0025322794901562. doi:10.1016/0025-3227(94)90156-2.

Bertin, X. (2005). *Morphodynamique séculaire, modélisation et architecture interne d'un système baie-embouchure tidale: le Pertuis de Maumusson et la Baie de Marennes-Oléron*. Ph.D. thesis La Rochelle. URL: http://www.theses.fr/2005LAROS140.

Bertin, X., & Chaumillon, r. (2005). Contribution of simulations on historical bathymetries to the understanding of evolutions of estuarine sand banks. *Comptes Rendus Geoscience*, *337*, 1375–1383. URL: http://www.sciencedirect.com/science/article/pii/S1631071305001768. doi:10.1016/j.crte.2005.06.007.

Bertin, X., Prouteau, E., & Letetrel, C. (2013). A significant increase in wave height in the North Atlantic Ocean over the 20th century. *Global and Planetary Change*, *106*, 77–83. URL: http://www.sciencedirect.com/science/article/pii/S092181811300088X. doi:10.1016/j.gloplacha.2013.03.009.

Biscara, L., Schmitt, T., Correard, S., & Creach, R. (2014). Modèles numériques de bathymétrie pour la prévision hydrodynamique du dispositif vigilance vagues-submersions. In *XIIIèmes JNGCGC Dunkerque* (pp. 547–556). Editions Paralia. URL: http://www.paralia.fr/jngcgc/13_60_biscara.pdf. doi:10.5150/jngcgc.2014.060.

Boudière, E., Maisondieu, C., Ardhuin, F., Accensi, M., Pineau-Guillou, L., & Lepesqueur, J. (2013). A suitable metocean hindcast database for the design of Marine energy converters. *International Journal of Marine Energy*, *3-4*, e40–e52. URL: http://www.sciencedirect.com/science/article/pii/S2214166913000362. doi:10.1016/j.ijome.2013.11.010.

Briquet, A. (1930). *Le littoral du nord de la France et son évolution morphologique*. Thèse de doctorat Université de Paris (1896-1968). Faculté des lettres France.

795 Brown, J. M., Amoudry, L. O., Souza, A. J., & Plater, A. J. (2015). Resid-
796 ual circulation modelled at national UK scale to identify sediment pathways
797 to inform coastal evolution models. In *The Proceedings of the Coastal Sedi-*
798 *ments 2015.The Proceedings of the Coastal Sediments 2015.* (p. 14). Wang,
799 P.; Rosati, J.D.; Cheng, J.,. URL: https://core.ac.uk/display/33454048.

800 Carter, R. W. G., Lowry, P., & Stone, G. W. (1982). Sub-tidal ebb-
801 shoal control of shoreline erosion via wave refraction, Magilligan fore-
802 land, Northern Ireland. *Marine Geology*, *48*, M17–M25. URL: http:
803 //www.sciencedirect.com/science/article/pii/0025322782901268.
804 doi:10.1016/0025-3227(82)90126-8.

805 Castelle, B., Marieu, V., Bujan, S., Splinter, K. D., Robinet, A., Sénéchal,
806 N., & Ferreira, S. (2015). Impact of the winter 2013-2014 series of severe
807 Western Europe storms on a double-barred sandy coast: Beach and dune
808 erosion and megacusp embayments. *Geomorphology*, *238*, 135–148. URL:
809 http://adsabs.harvard.edu/abs/2015Geomo.238..135C. doi:10.1016/j.
810 geomorph.2015.03.006.

811 Caston, V. N. D. (1972). Linaer sand banks in the Southern North Sea. *Sedi-*
812 *mentology*, *18*, 63–78. doi:10.1111/j.1365-3091.1972.tb00003.x.

813 CEREMA (1985). Centre d'Archivage National de Données de Houles In
814 Situ Littoral de la France métropolitaine - CANDHIS 1985. URL: http:
815 //candhis.cetmef.developpement-durable.gouv.fr/.

816 CEREMA (2018). *Dynamiques et évolution du littoral Synthèse des*
817 *connaissances de la frontière Belge à la pointe du Hourdel*. Fasci-
818 cule 1. URL: http://www.cerema.fr/fr/centre-ressources/boutique/
819 dynamiques-evolution-du-littoral.

820 Chaverot, S. (2006). *Impact des variations récentes des conditions météo-*
821 *marines sur les littoraux meubles du Nord-Pas-de-Calais*. thesis Université
822 Littoral Côte d'Opale. URL: http://www.theses.fr/2006DUNK0146.

Chaverot, S., Héquette, A., & Cohen, O. (2008). Changes in storminess and shoreline evolution along the northern coast of France during the second half of the 20th century. *Annales de Géomorphologie / Annals of Geomorphology / Zeitschrift für Geomorphologie*, *Sup. Bd.,52*, Sup. Bd., 52 (3), p. 1–20. URL: https://www.schweizerbart.de/papers/zfg_suppl/detail/52/65699/Changes_in_storminess_and_shoreline_evolution_along_the_northern_coast_of_France_during_the_second_half_of_the_20th_century. doi:10.1127/0372-8854/2008/0052S3-0001.

Cooper, J. A. G., Jackson, D. W. T., Navas, F., McKenna, J., & Malvarez, G. (2004). Identifying storm impacts on an embayed, high-energy coastline: examples from western Ireland. *Marine Geology*, *210*, 261–280. URL: http://www.sciencedirect.com/science/article/pii/S0025322704001409. doi:10.1016/j.margeo.2004.05.012.

Cooper, J. a. G., & Navas, F. (2004). Natural bathymetric change as a control on century-scale shoreline behavior. *Geology*, *32*, 513–516. URL: https://pubs.geoscienceworld.org/gsa/geology/article-abstract/32/6/513/29467/natural-bathymetric-change-as-a-control-on-century. doi:10.1130/G20377.1.

Corbau, C. (1995). *Dynamique sédimentaire en domaine Macrotidale : exemple du littoral du Nord de la France (Dunkerque)*. Ph.D. thesis Université des Sciences et Technologiques de Lille 1.

Corbau, C., Tessier, B., & Chamley, H. (1999). Seasonal Evolution of Shoreface and Beach System Morphology in a Macrotidal Environment, Dunkerque Area, Northern France. *Journal of Coastal Research*, *15*. URL: http://journals.fcla.edu/jcr/article/view/80429.

Crapoulet, A. (2015). *Evolution du trait de côte, bilan sédimentaire et évaluation des zones à risques sur le littoral du Nord-Pas-de-Calais : analyse multi-échelles par LiDAR aéroporté*. Ph.D. thesis Université du Littoral Côte d'Opale.

Crapoulet, A., Héquette, A., Marin, D., Levoy, F., & Bretel, P. (2017). Variations in the response of the dune coast of northern France to major storms as a function of available beach sediment volume. *Earth Surface Processes and Landforms*, *42*, 1603–1622. URL: https://onlinelibrary.wiley.com/doi/abs/10.1002/esp.4098. doi:10.1002/esp.4098.

Davidson, M. A., O'Hare, T. J., & George, K. J. (2008). Tidal Modulation of Incident Wave Heights: Fact or Fiction? *Journal of Coastal Research*, *24*, 151–159. URL: https://www.jcronline.org/doi/abs/10.2112/06-0754.1. doi:10.2112/06-0754.1.

Davidson-Arnott, R., & N. Law, M. (1996). *Measurement and prediction of long-term sediment supply to Coastal Foredunes* volume 12.

Davies, J. L. (1980). *Geographical variation in coastal development*. Longman Sc & Tech.

De Moor, G. (2002). Evaluation of sea-floor sediment dynamics in the Flemish Banks (southern North Sea) between 1985 and 1995. *Géomorphologie : relief, processus, environnement*, *8*, 135–150. URL: https://www.persee.fr/doc/morfo_1266-5304_2002_num_8_2_1135. doi:10.3406/morfo.2002.1135.

Deleu, S., Van Lancker, V., Van den Eynde, D., & Moerkerke, G. (2004). Morphodynamic evolution of the kink of an offshore tidal sandbank: the Westhinder Bank (Southern North Sea). *Continental Shelf Research*, *24*, 1587–1610. URL: http://www.sciencedirect.com/science/article/pii/S027843430400161X. doi:10.1016/j.csr.2004.07.001.

Dewez, S., Clabaut, P., Vicaire, O., Beck, C., Chamley, H., & Augris, C. (1989). Transits sedimentaires resultants aux confins Manche-mer du Nord. *Bulletin de la Société Géologique de France*, *V*, 1043–1053. URL: https://pubs-geoscienceworld-org.insu.bib.cnrs.fr/sgf/bsgf/article/V/5/1043/90299/transits-sedimentaires-resultants-aux-confins. doi:10.2113/gssgfbull.V.5.1043.

Dodet, G., Bertin, X., & Taborda, R. (2010). Wave climate variability in the North-East Atlantic Ocean over the last six decades. *Ocean Modelling*, *31*, 120–131. URL: http://www.sciencedirect.com/science/article/pii/S1463500309002066. doi:10.1016/j.ocemod.2009.10.010.

Dyer, K. R., & Huntley, D. A. (1999). The origin, classification and modelling of sand banks and ridges. *Continental Shelf Research*, *19*, 1285–1330. URL: http://www.sciencedirect.com/science/article/pii/S027843439900028X. doi:10.1016/S0278-4343(99)00028-X.

EGIS (2014). *Etude de faisabilité pour le réensablement de la partie centrale de la baie de Wissant - Phase 1: Dimensionnement du réensablement - Elaboration de scénarios de réensablement*. Rapport définitif EP 132771M. URL: https://www.hauts-de-france.developpement-durable.gouv.fr/IMG/pdf/ep132771m_wissant_phase1_vfinale.pdf.

Garlan, T. (1990). L'apport des levés bathymétriques pour la connaissance de la dynamique sédimentaire. L'exemple des Ridens de la Rade aux abords de Calais. (pp. 71–75). Marseille.

Giardino, A., Van den Eynde, D., & Monbaliu, J. (2010). Wave effects on the morphodynamic evolution of an offshore sand bank. *Journal of Coastal Research*, (pp. 127–140). URL: http://agris.fao.org/agris-search/search.do?recordID=AV2012056824. doi:10.2307/40928825.

Hanna, J. E., & Cooper, J. (2002). Mesoscale Morphological Changes on Linear, Nearshore Sandbanks, Co.Wexford, SE Ireland. *Journal of Coastal Research*, (pp. 356–364). URL: http://www.bioone.org/doi/abs/10.2112/1551-5036-36.sp1.356. doi:10.2112/1551-5036-36.sp1.356.

Hédou, F., Roche, A., Trmal, C., Moraud, S., & Deniaud, Y. (2018). Élaboration de l'indicateur national de l'érosion côtière. In *XVèmes Journées, La Rochelle* (pp. 647–654). Editions Paralia. URL: http://www.paralia.fr/jngcgc/15_75_hedou.pdf. doi:10.5150/jngcgc.2018.075.

Hedges, T. (2015). Combinations of waves and currents: an introduction. *Proceedings of the Institution of Civil Engineers*, *Part 1*, 567–585. doi:10.1680/iicep.1987.319.

Hervouet, J.-M. (2007). *Hydrodynamics of Free Surface Flows: Modelling With the Finite Element Method*. Wiley; 1 edition (May 29, 2007).

Hesp, P. (1988). *Surfzone, beach and fordune interactions on the Australian southeast coast* volume 3.

Horrillo-Caraballo, J. M., & Reeve, D. E. (2008). Morphodynamic behaviour of a nearshore sandbank system: The Great Yarmouth Sandbanks, U.K. *Marine Geology*, *254*, 91–106. URL: http://www.sciencedirect.com/science/article/pii/S002532270800176X. doi:10.1016/j.margeo.2008.05.014.

Houbolt, J. (1968). Recent sediments in the Southern Bight of the North Sea. *Geologie en Mijnbouw 47*, .

Houser, C., Hapke, C., & Hamilton, S. (2008). Controls on coastal dune morphology, shoreline erosion and barrier island response to extreme storms. *Geomorphology*, (pp. 223–240). URL: https://scholar.uwindsor.ca/environmentalsciencepub/31. doi:10.1016/j.geomorph.2007.12.007.

Héquette, A., & Aernouts, D. (2010). The influence of nearshore sand bank dynamics on shoreline evolution in a macrotidal coastal environment, Calais, Northern France. *Continental Shelf Research*, *30*, 1349–1361. URL: http://www.sciencedirect.com/science/article/pii/S0278434310001561. doi:10.1016/j.csr.2010.04.017.

Héquette, A., Anthony, E. J., Ruz, M.-H., Maspataud, A., Aernouts, D., & Hemdane, Y. (2013). The influence of nearshore sand banks on coastal hydrodynamics and sediment transport, northern coast of France. In *Proceedings Coastal Dynamics* (pp. 801–810).

Héquette, A., Hemdane, Y., & Anthony, E. J. (2008). Sediment transport under wave and current combined flows on a tide-

dominated shoreface, northern coast of France. *Marine Geology*, *249*, 226–242. URL: http://www.sciencedirect.com/science/article/pii/S0025322707003027. doi:10.1016/j.margeo.2007.12.003.

Héquette, A., Ruz, M. H., Maspataud, A., & Sipka, V. (2009). Effects of nearshore sand bank and associated channel on beach hydrodynamics: implications for beach and shoreline evolution. *Journal of Coastal Research*, *Special issue 56*, 59–63. URL: http://www.jstor.org/stable/25737537.

Huthnance, J. M. (1982). On one mechanism forming linear sand banks. *Estuarine, Coastal and Shelf Science*, *14*, 79–99. URL: http://www.sciencedirect.com/science/article/pii/S0302352482800686. doi:10.1016/S0302-3524(82)80068-6.

Idier, D., Paris, F., Cozannet, G. L., Boulahya, F., & Dumas, F. (2017). Sea-level rise impacts on the tides of the European Shelf. *Continental Shelf Research*, *137*, 56–71. URL: http://www.sciencedirect.com/science/article/pii/S0278434317300250. doi:10.1016/j.csr.2017.01.007.

Jing, L., & Ridd, P. V. (1996). Wave-current bottom shear stresses and sediment resuspension in Cleveland Bay, Australia. *Coastal Engineering*, *29*, 169–186. URL: http://www.sciencedirect.com/science/article/pii/S0378383996000233. doi:10.1016/S0378-3839(96)00023-3.

Kenyon, N. H., Belderson, R. H., Stride, A. H., & Johnson, M. A. (1981). Offshore Tidal Sand-Banks as Indicators of Net Sand Transport and as Potential Deposits. In *Holocene Marine Sedimentation in the North Sea Basin* (pp. 257–268). Wiley-Blackwell. URL: https://onlinelibrary.wiley.com/doi/abs/10.1002/9781444303759.ch20. doi:10.1002/9781444303759.ch20.

King, E. V., Conley, D. C., Masselink, G., Leonardi, N., McCarroll, R. J., & Scott, T. (2019). The Impact of Waves and Tides on Residual Sand Transport on a Sediment-Poor, Energetic, and Macrotidal Continental Shelf. *Journal of Geophysical Research: Oceans*, *124*,

964 4974–5002. URL: https://agupubs.onlinelibrary.wiley.com/doi/abs/
965 10.1029/2018JC014861. doi:10.1029/2018JC014861.

966 Lanckneus, J., De Moor, G., De Schaepmeester, G., De Winne, E., & Meyus,
967 I. (1992). Monitoring of a tidal sandbank: evolution of bedforms, volumetric
968 trends, sedimentological changes. *Special Publication (Hydrographic Society)*,
969 .

970 Lanckneus, J., De Moor, G., & Stolk, A. (1994). Environmental set-
971 ting, morphology and volumetric evolution of the Middelkerke Bank
972 (southern North Sea). *Marine Geology*, *121*, 1–21. URL: http:
973 //www.sciencedirect.com/science/article/pii/0025322794901538.
974 doi:10.1016/0025-3227(94)90153-8.

975 Latapy, A., Héquette, A., Pouvreau, N., Weber, N., & Robin-Chanteloup, J.-
976 B. (2019). Mesoscale Morphological Changes of Nearshore Sand Banks since
977 the Early 19th Century, and Their Influence on Coastal Dynamics, Northern
978 France. *Journal of Marine Science and Engineering*, *7*, 73. URL: https:
979 //www.mdpi.com/2077-1312/7/3/73. doi:10.3390/jmse7030073.

980 Le Roy, R., & Simon, B. (2003). *Réalisation et validation d'un modèle de marée*
981 *en Manche et dans le Golfe de Gascogne (application à la réalisation d'un*
982 *nouveau programme de réduction des sondages bathymétriques)*. Technical
983 Report 002/03 EPSHOM.

984 Li, D., Tang, C., Hou, X., & Zhang, H. (2019). Rapid Morphological Changes
985 Caused by Intensive Coastal Development in Longkou Bay, China. *Journal of*
986 *Coastal Research*, . URL: http://www.jcronline.org/doi/abs/10.2112/
987 JCOASTRES-D-18-00095.1. doi:10.2112/JCOASTRES-D-18-00095.1.

988 Lugo-Fernández, A., Roberts, H. H., & Wiseman, J., W. J. (1998). Tide Effects
989 on Wave Attenuation and Wave Set-up on a Caribbean Coral Reef. *Estuarine,*
990 *Coastal and Shelf Science*, *47*, 385–393. URL: http://www.sciencedirect.
991 com/science/article/pii/S0272771498903651. doi:10.1006/ecss.1998.
992 0365.

MacDonald, N. J., & O'Connor, B. A. (1996). Changes in wave impact on the Flemish coast due to increased mean sea level. *Journal of Marine Systems*, *7*, 133–144. URL: http://www.sciencedirect.com/science/article/pii/0924796395000321. doi:10.1016/0924-7963(95)00032-1.

Marcos, F. (2003). Logiciel TOMAWAC de Propagation de Houle En Elements Finis. Notice D'utilisation, Version 5.2, .

Masselink, G. (1998). The effect of sea breeze on beach morphology, surf zone hydrodynamics and sediment resuspension. *Marine Geology*, *146*, 115–135. URL: http://www.sciencedirect.com/science/article/pii/S0025322797001217. doi:10.1016/S0025-3227(97)00121-7.

Masselink, G., Austin, M., Scott, T., Poate, T., & Russell, P. (2014). Role of wave forcing, storms and NAO in outer bar dynamics on a high-energy, macro-tidal beach. *Geomorphology*, *226*, 76–93. URL: https://linkinghub.elsevier.com/retrieve/pii/S0169555X14003900. doi:10.1016/j.geomorph.2014.07.025.

Mattheus, C., Diggins, T., Boyce, C., Cockrell, J., Kruske, M., & VanWinkle, M. (2018). Geomorphology of a Harbor-Breakwater Beach along a High Sand-Supply, Wave-Dominated Great Lakes Littoral Cell. *Journal of Coastal Research*, . URL: http://www.jcronline.org/doi/abs/10.2112/JCOASTRES-D-17-00209.1. doi:10.2112/JCOASTRES-D-17-00209.1.

McNinch, J. E. (2004). Geologic control in the nearshore: shore-oblique sandbars and shoreline erosional hotspots, Mid-Atlantic Bight, USA. *Marine Geology*, *211*, 121–141. URL: http://www.sciencedirect.com/science/article/pii/S0025322704002075. doi:10.1016/j.margeo.2004.07.006.

Michaud, H., Pasquet, A., Baraille, R., Leckler, F., Aouf, L., Dalphinet, A., Huchet, M., Roland, A., Dutour-Sikiric, M., Ardhuin, F., & Filipot, J. F. (2015). Implementation of the new French operational coastal wave forecasting system and application to a wave- current interaction study. (p. 10). Key West, Florida.

Morton, R. A., Gibeaut, J. C., & Paine, J. G. (1995). Meso-scale transfer of sand during and after storms: implications for prediction of shoreline movement. *Marine Geology*, *126*, 161–179. URL: http://www.sciencedirect.com/science/article/pii/0025322795000716. doi:10.1016/0025-3227(95)00071-6.

Osuna, P., & Monbaliu, J. (2004). Wave–current interaction in the Southern North Sea. *Journal of marine systems*, *52*, 65–87. doi:10.1016/j.jmarsys.2004.03.002.

Pan, S., MacDonald, N., Williams, J., O'Connor, B. A., Nicholson, J., & Davies, A. M. (2007). Modelling the hydrodynamics of offshore sandbanks. *Continental Shelf Research*, *27*, 1264–1286. URL: http://www.sciencedirect.com/science/article/pii/S0278434307000337. doi:10.1016/j.csr.2007.01.007.

Parker, G., Lanfredi, N. W., & Swift, D. J. P. (1982). Seafloor response to flow in a southern hemisphere sand-ridge field: Argentine inner shelf. *Sedimentary Geology*, *33*, 195–216. URL: http://www.sciencedirect.com/science/article/pii/0037073882900550. doi:10.1016/0037-0738(82)90055-0.

Peregrine, D. H. (1976). Interaction of Water Waves and Currents. In C.-S. Yih (Ed.), *Advances in Applied Mechanics* (pp. 9–117). Elsevier volume 16. URL: http://www.sciencedirect.com/science/article/pii/S0065215608700875. doi:10.1016/S0065-2156(08)70087-5.

Pintat, J.-F. (1975). *Projet de loi relatif à la prospection, à la recherche et à l'exploitation des substances minérales non visées par l'article 2 du code minier et contenues dans les fonds marins du domaine public métropolitain*. Technical Report 381 Sénat.

Reichmüth, B., & Anthony, E. J. (2007). Tidal influence on the intertidal bar morphology of two contrasting macrotidal beaches. *Geomorphology*, *90*, 101–114. URL: http://www.sciencedirect.com/science/article/pii/S0169555X0700030X. doi:10.1016/j.geomorph.2007.01.015.

Ruz, M.-H., Héquette, A., Marin, D., Sipka, V., Crapoulet, A., & Cartier, A. (2017). Development of an incipient foredune field along a prograding macrotidal shoreline, northern France. *Géomorphologie : relief, processus, environnement*, *23*, 37–50. URL: http://journals.openedition.org/geomorphologie/11638. doi:10.4000/geomorphologie.11638.

Schmitt, T., & Mitchell, N. C. (2014). Dune-associated sand fluxes at the nearshore termination of a banner sand bank (Helwick Sands, Bristol Channel). *Continental Shelf Research*, *76*, 64–74. URL: http://www.sciencedirect.com/science/article/pii/S0278434314000089. doi:10.1016/j.csr.2014.01.003.

Scott, T., Masselink, G., & Russell, P. (2011). Morphodynamic characteristics and classification of beaches in England and Wales. *Marine Geology*, *286*, 1–20. URL: http://www.sciencedirect.com/science/article/pii/S0025322711001095. doi:10.1016/j.margeo.2011.04.004.

Sedrati, M., & Anthony, E. J. (2007). Storm-generated morphological change and longshore sand transport in the intertidal zone of a multi-barred macrotidal beach. *Marine Geology*, *244*, 209–229. URL: http://www.sciencedirect.com/science/article/pii/S0025322707001776. doi:10.1016/j.margeo.2007.07.002.

Sedrati, M., & Anthony, E. J. (2014). Confronting coastal morphodynamics with counter-erosion engineering: the emblematic case of Wissant Bay, Dover Strait. *Journal of Coastal Conservation*, *18*, 483–494. URL: https://doi.org/10.1007/s11852-013-0300-1. doi:10.1007/s11852-013-0300-1.

Shaw, J., Duffy, G., Taylor, R. B., Chassé, J., & Frobel, D. (2008). Role of a Submarine Bank in the Long-Term Evolution of the Northeast Coast of Prince Edward Island, Canada. *Journal of Coastal Research*, (pp. 1249–1259). URL: http://www.jcronline.org/doi/abs/10.2112/07-08607.1. doi:10.2112/07-08607.1.

Shom (2017). *Annuaire des Marées 2019, Ports de France Métropole, Tome 1*.

Short, A. D. (Ed.) (1999). *Handbook of beach and shoreface morphodynamics*. New York: John Wiley.

Soulsby, R. (1997). *Dynamics of Marine Sands: A Manual for Practical Applications*. Thomas Telford.

Soulsby, R. L. (1983). Chapter 5 The Bottom Boundary Layer of Shelf Seas. In B. Johns (Ed.), *Elsevier Oceanography Series* (pp. 189–266). Elsevier volume 35 of *Physical Oceanography of Coastal and Shelf Seas*. URL: http://www.sciencedirect.com/science/article/pii/S0422989408705038. doi:10.1016/S0422-9894(08)70503-8.

de Swart, H. E., & Yuan, B. (2018). Dynamics of offshore tidal sand ridges, a review. *Environmental Fluid Mechanics*, . URL: https://doi.org/10.1007/s10652-018-9630-8. doi:10.1007/s10652-018-9630-8.

Tessier, B., Corbau, C., Chamley, H., & Auffret, J.-P. (1999). Internal Structure of Shoreface Banks Revealed by High-Resolution Seismic Reflection in a Macrotidal Environment (Dunkerque Area, Northern France). *Journal of Coastal Research*, *15*, 593–606. URL: http://www.jstor.org/stable/4298976.

Thomas, T., Phillips, M. R., Williams, A. T., & Jenkins, R. E. (2011). A multi-century record of linked nearshore and coastal change. *Earth Surface Processes and Landforms*, *36*, 995–1006. URL: http://onlinelibrary.wiley.com.insu.bib.cnrs.fr/doi/10.1002/esp.2127/abstract. doi:10.1002/esp.2127.

Vicaire, O. (1991). *Dynamique hydro-sédimentaire en mer du Nord mériodionale (du Cap Blanc-Nez à la frontière Belge)*. Ph.D. thesis Université des Sciences et Techniques de Lille 1.

Villaret, C., & Davies, A. G. (2004). Numerical modelling of littoral sand transport. In *Proceedings of the 29th International Conference on Coastal Engineering* (pp. 1678–1689.). Lisbon: World Scientific.

Wolf, J., & Prandle, D. (1999). Some observations of wave–current interaction. *Coastal Engineering*, *37*, 471–485. URL: http://www.sciencedirect.com/science/article/pii/S0378383999000393. doi:10.1016/S0378-3839(99)00039-3.

Wright, L. D., & Short, A. D. (1984). Morphodynamic variability of surf zones and beaches: A synthesis. *Marine Geology*, *56*, 93–118. URL: http://www.sciencedirect.com/science/article/pii/0025322784900082. doi:10.1016/0025-3227(84)90008-2.

Young, I. R., Zieger, S., & Babanin, A. V. (2011). Global Trends in Wind Speed and Wave Height. *Science*, *332*, 451–455. URL: https://science.sciencemag.org/content/332/6028/451. doi:10.1126/science.1197219.

Zijlema, M., van Vledder, G. P., & Holthuijsen, L. H. (2012). Bottom friction and wind drag for wave models. *Coastal Engineering*, *65*, 19–26. URL: http://www.sciencedirect.com/science/article/pii/S0378383912000440. doi:10.1016/j.coastaleng.2012.03.002.

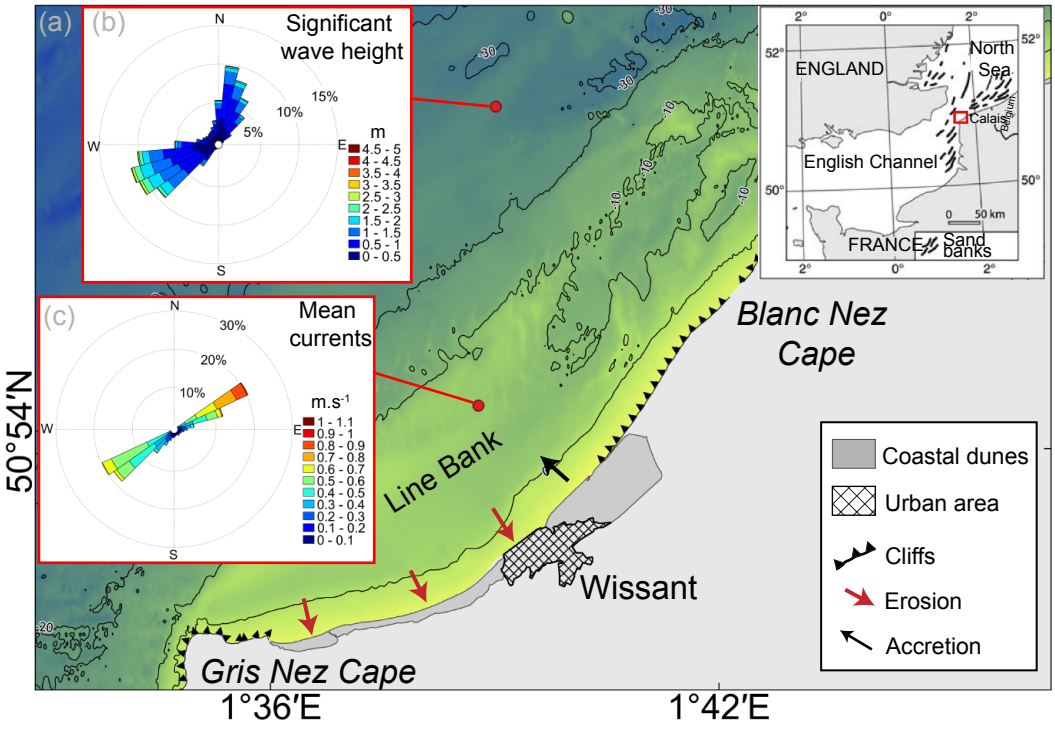

Figure 1: Wissant bay in the southern North Sea facing the Dover Strait (inset map) (a) Bathymetry from HOMONIM Digital Elevation Model (`http://dx.doi.org/10.17183/MNT_ATL100m_HOMONIM_WGS84`) and synthesis of Wissant bay's shoreline evolution (Chaverot, 2006; Crapoulet, 2015), (b) Wave height from the HOMERE database (point E164N5094) and (c) direction and intensity of mean currents during the campaign between 05/17/2016 and 06/07/2016 (DDTM62)

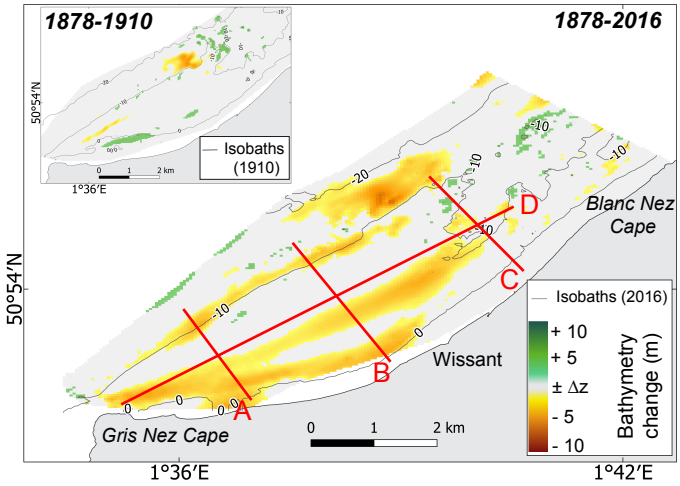

Figure 2: Bathymetric differential map of the Wissant bay between 1878 and 2016 and between 1878 and 1910 (inset map). Red-orange pattern indicates a seabed lowering; reciprocally blue-green areas correspond to vertical accretion; areas in grey correspond to the margin error ($\pm\Delta z$) and are considered as stable over the study period. Transects A, B, C and D correspond to the location of bathymetric profiles in Figure 3.

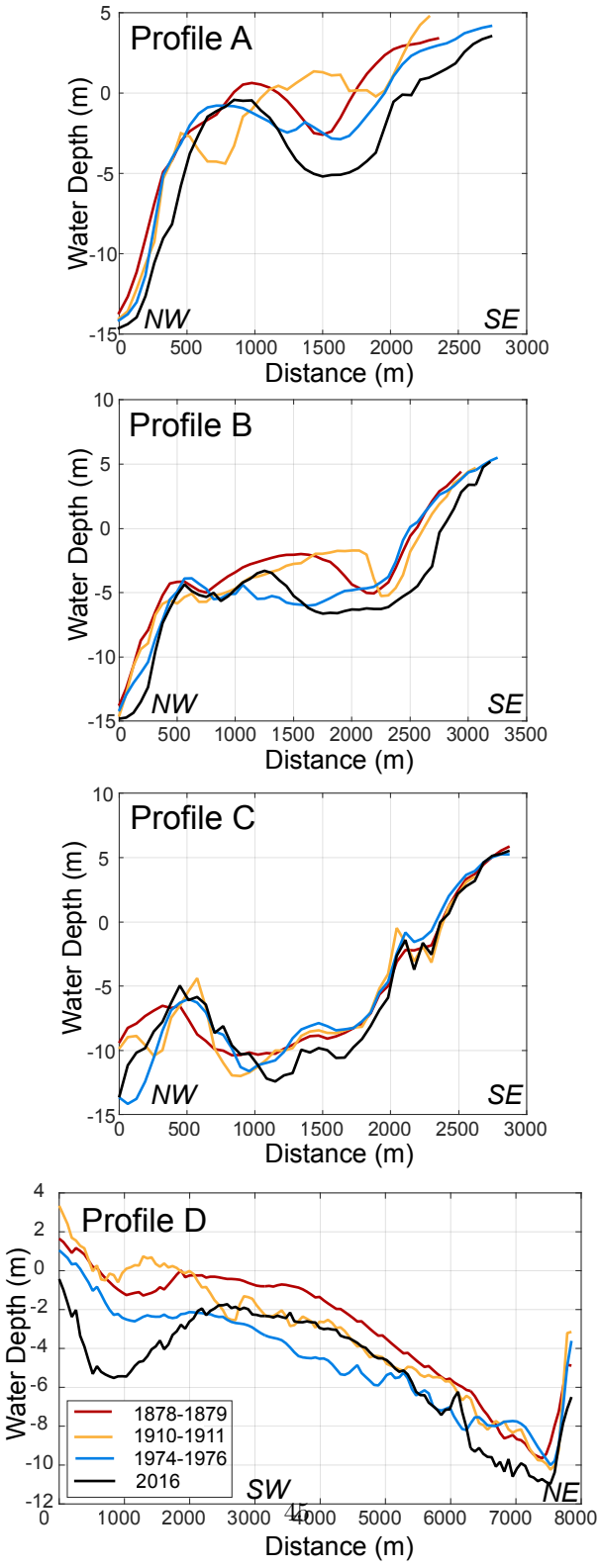

Figure 3: Bathymetry profiles evolution across the Wissant bay and the Line Bank from 1878 to 2016, (a-c) are cross-shore profiles and (d) is long-shore profile. See Figure 2 for profile location

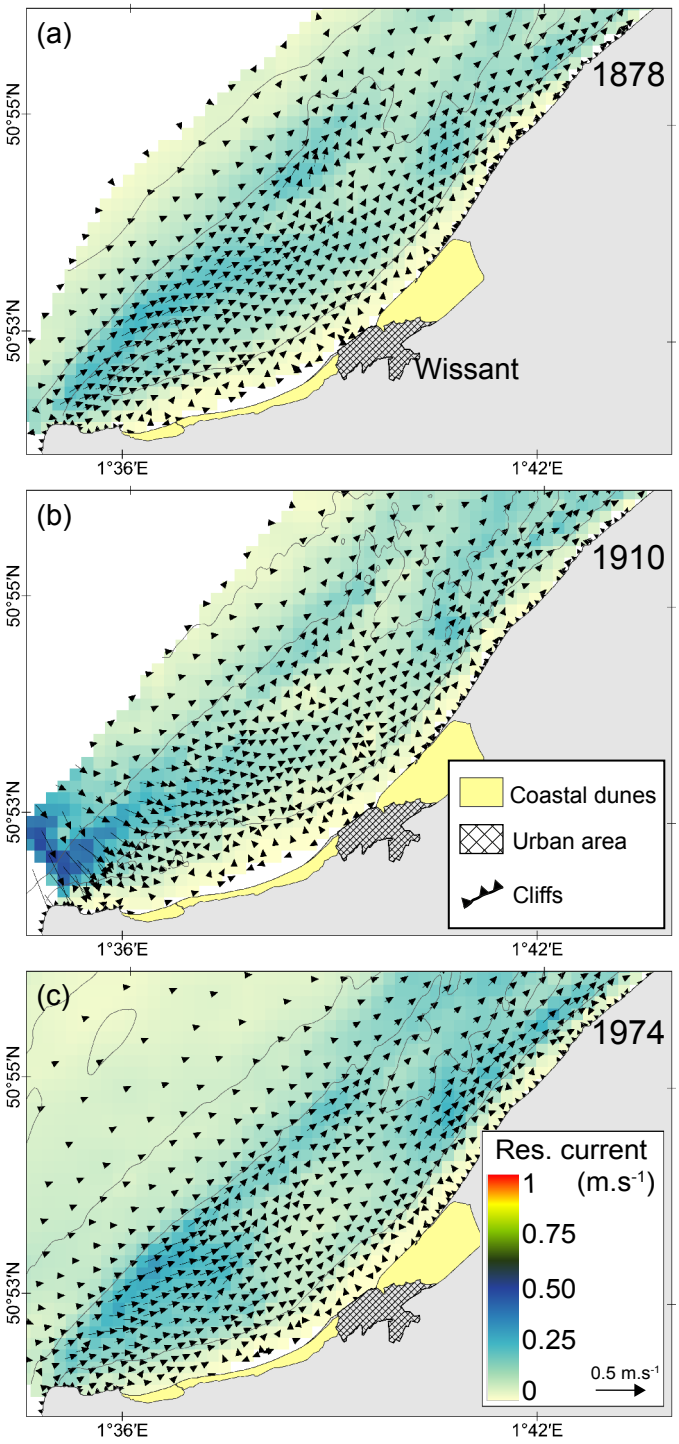

Figure 4: Simulations of changes in tidal residual current over 1878 (a), 1910 (b), and 1974 (c) bathymetries considering only the effect of tides.

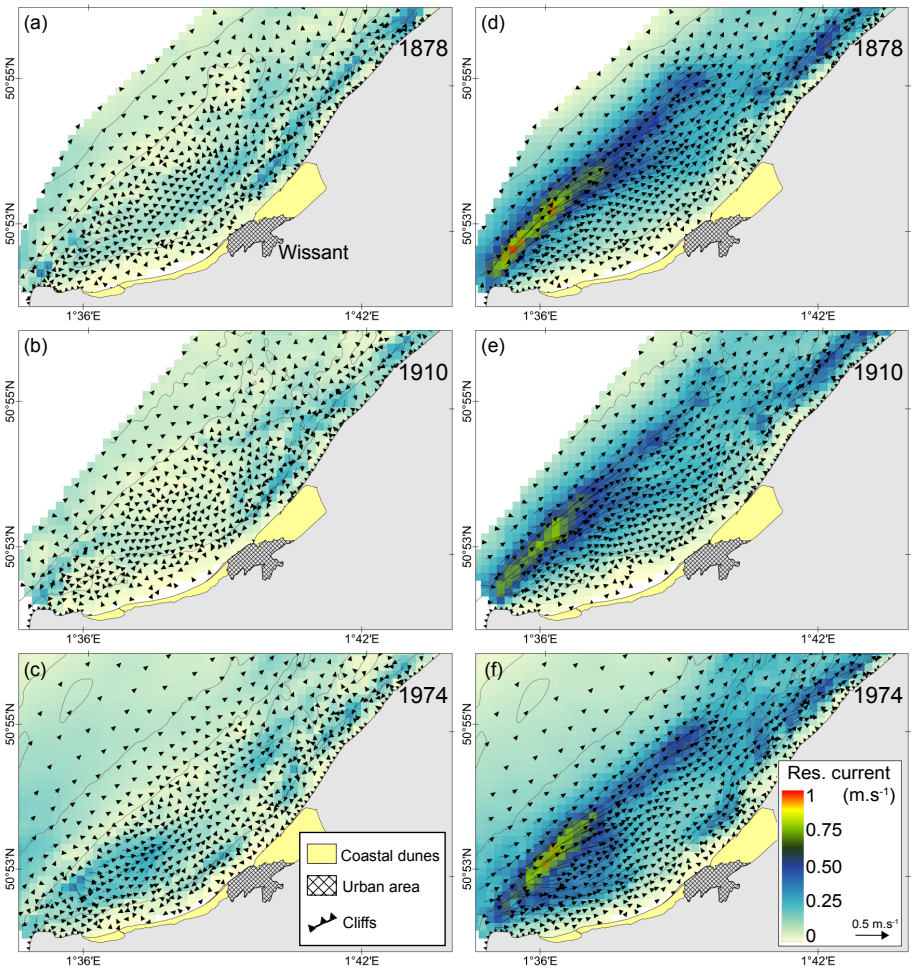

Figure 5: Simulations of changes in tidal residual current over 1878, 1910, and 1974 bathymetries considering the coupling effect of tides and waves: (a),(b), and (c) with north-easterly off-shore waves and (d), (e), and (f) with westerly off-shore waves

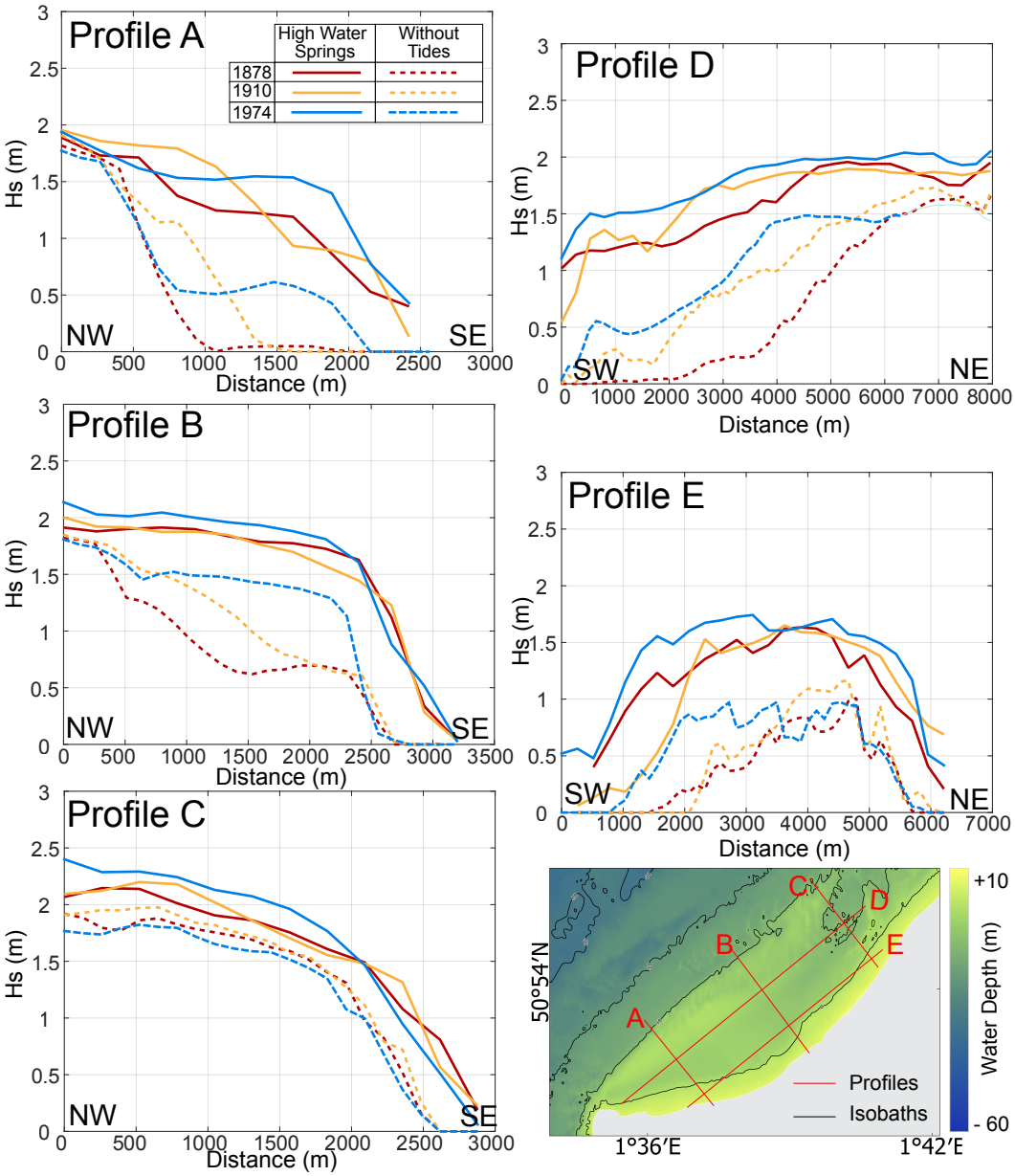

Figure 6: Significant wave height transects from the 1878, 1910 and 1974 models with north-easterly waves with and without considering tides

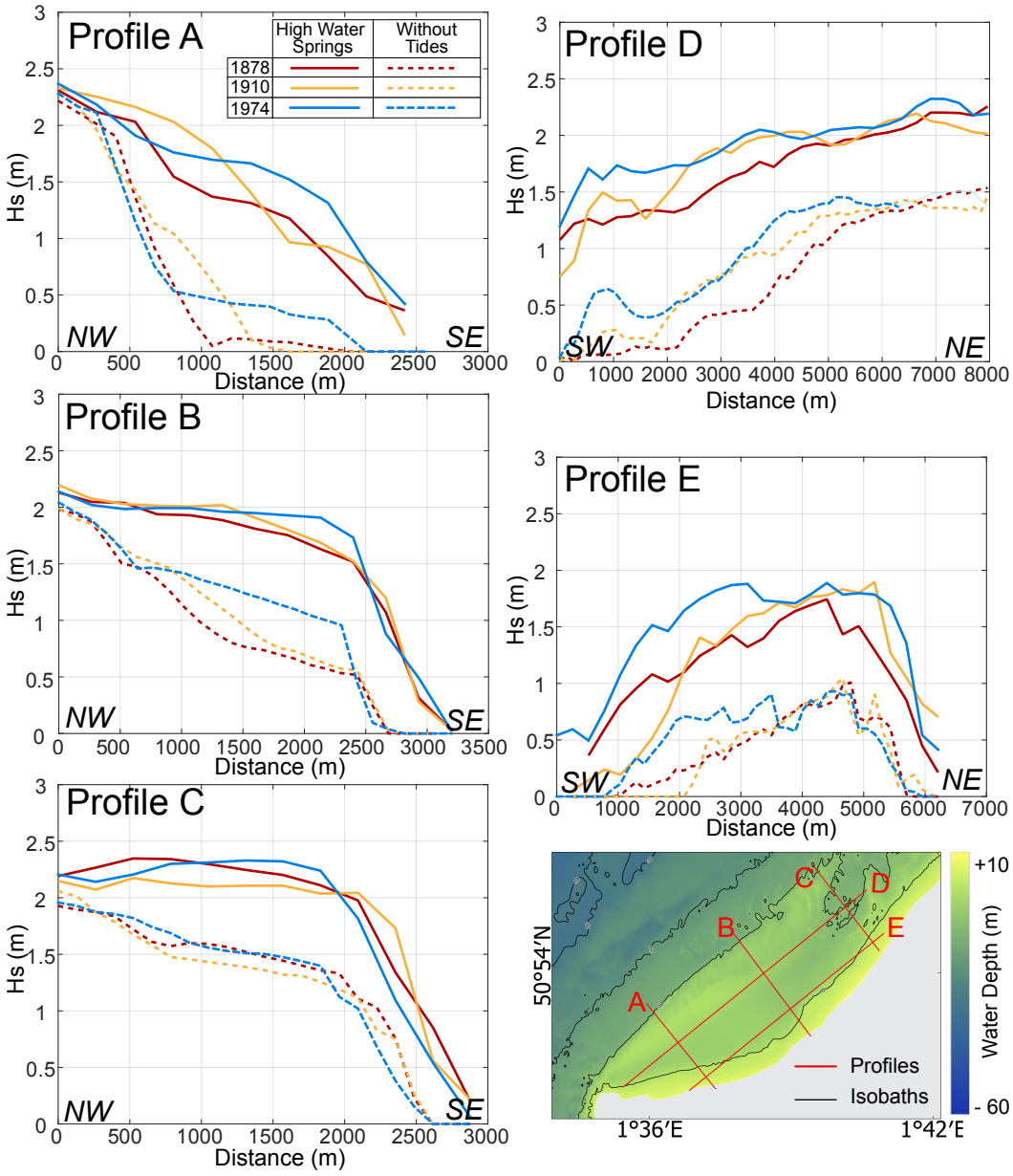

Figure 7: Significant wave height transects from the 1878, 1910 and 1974 models with westerly waves with and without considering tides

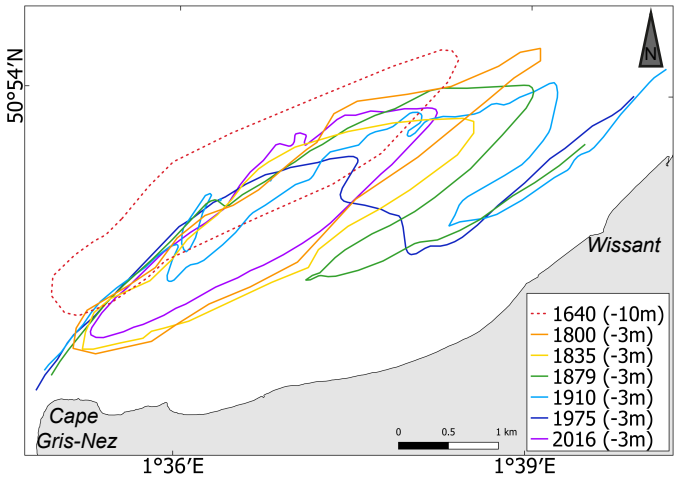

Figure 8: Evolution of the Line bank position and shape since 1640, adapted from the work of Briquet (1930)and completed with data digitized through this study. The -3m isobath was used as a reference for the position of the Line bank except for 1640 where the -10m isobath was chosen

.

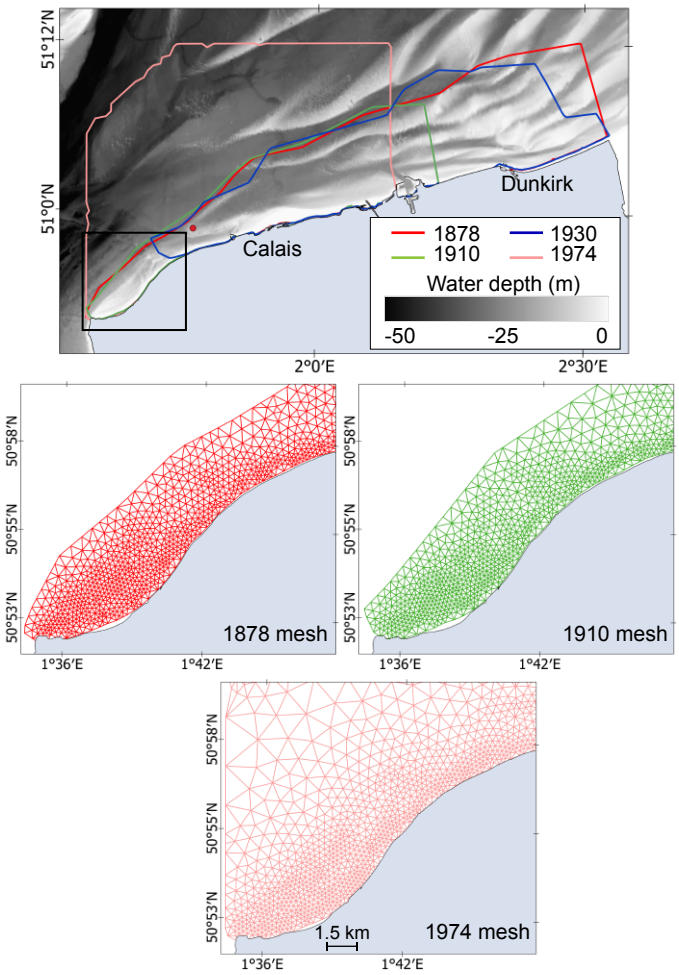

Figure 9: Above: Spatial extent of the 4 models used in this study on the HOMONIM Digital Elevation Model (`http://dx.doi.org/10.17183/MNT_ATL100m_HOMONIM_WGS84`), the black box indicates the location of the Wissant bay and the red dot the position of the currentmeter used for current validation in the Figure 10 . Bottom: zoom on meshes covering Wissant Bay (1878, 1910, 1974)

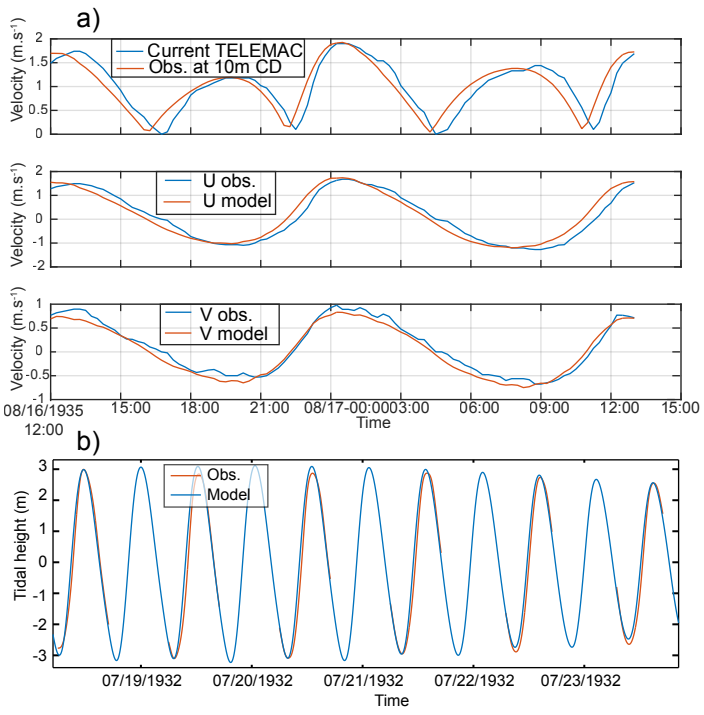

Figure 10: a) Tidal current observation made in 1935 and obtained with the 1930 model, offshore of Calais, at 10 m below Chart Datum (position of the currentmeter is indicated on the Figure 9). b) Comparison between tidal height observation at Calais in 1932 and tidal height obtained with the 1930 model at the same dates.

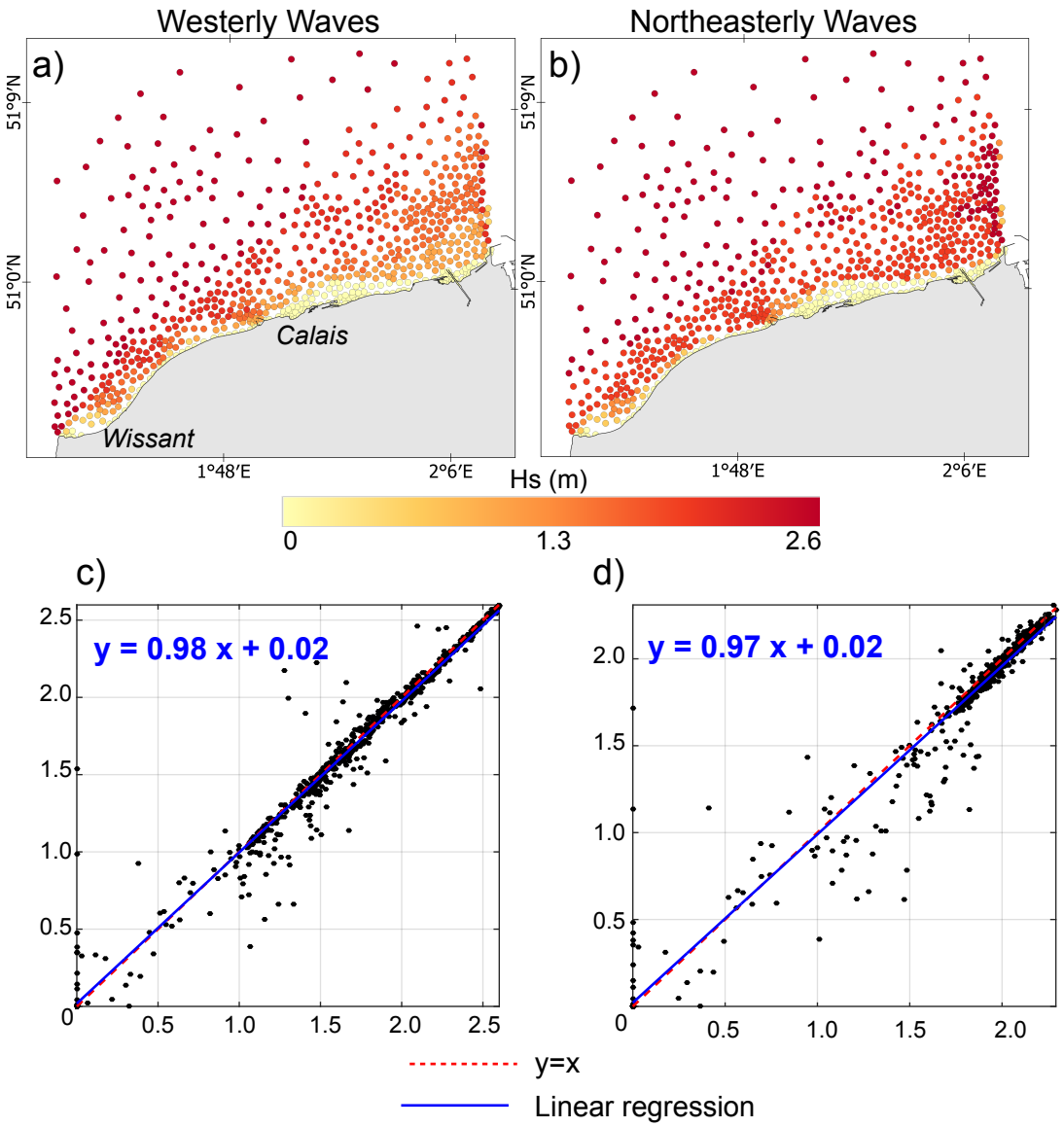

Figure 11: Wave height (Hs) obtained with the HOMONIM DEM with Tomawac for westerly (a) and northeasterly (b) off-shore waves. Q-Q plot comparing at each node Hs obtained with Tomawac and WaveWatch3 for westerly (c) et northeasterly waves (d). For both Q-Q plot linear regression (in blue) is plotted

Year	**1878-79**	**1910–11**	**1974–76**	**2016**
Surface (km^2)	691	400	1025	41
MHE (m)	15.5	15.5	10	3
MVE (m)	2.0	2.0	1.2	0.6

Table 1: Bathymetry surveys used in this study (source: SHOM, except for 2016 made by DDTM). MHE: Maximum Horizontal Error; MVE: Maximum Vertical Error. These first three bathymetry surveys were used for numerical modelling

Dates	**Nodes**	**Finite elements**
1878	8,058	15,698
1910	5,690	10,961
1974	4,408	8,559

Table 2: Computational mesh characteristics. Note that the year of each grid corresponds to the first year of the bathymetry surveys

NNE waves (Dir=N10)	WSW waves (Dir=N250)
Hs99% = 2.25m Fpeak99%=0,1364 Hz (Tpeak=7.33s)	Hs99% = 2.62m Fpeak99%=0,1336Hz (Tpeak=7.33s)

Table 3: 99th percentile of Hs and fpeak for WSW and NNE waves calculated from the HOMERE database (`http://doi.org/10.12770/cf47e08d-1455-4254-955e-d66225c9dc90`)

	1878-1910	1910-1974	**1878-1974**
Western foreshore	Hs ↓	Hs ↑	**Overall increase**
Central foreshore	Hs ↑	Hs ↑	**Overall increase**
Eastern foreshore	Hs ↓ or remained stable	Hs ↓ or remained stable	**Stable**
Line bank	Hs ↑ or remained stable	Hs ↑	**Increase**
Coastal channel	Hs ↓ or remained stable	Hs ↑	**Increase**

Table 4: Synthesis of wave height evolution depending on the location in the bay and the period considered

		1878	1910	1930	1974
Calais	Obs	**0.87**	**0.92**	**0.92**	**0.83**
R²		0.67	0.51	0.51	0.79
RMSE	Pred	**0.92**	**0.92**	**0.93**	**0.88**
		0.50	0.54	0.48	0.68
Dunkirk	Obs	**0.91**	-	**0.88**	-
R²		0.43		0.54	
RMSE	Pred	**0.92**	-	**0.88**	-
		0.43		0.55	

Table 5: Statistic computed (R^2 and RMSE) by comparing simulated tidal height at Calais and Dunkirk from each model with observations and predictions

NNE waves WW3 (Dir=10°N)	WSW waves WW3 (Dir=230°N)
21/03/2015 22:00 Hs= 2.2 m Fpeak99%=0,14 Hz (Tpeak=7.14s)	*22/02/2015 23:00* Hs = 2.5 m Fpeak99%=0,14Hz (Tpeak=7.14s)

Table 6: WaveWatch3 outputs used to validate TOMAWAC runs